AD-A077 570 MCDONNELL DOUGLAS ASTRONAUTICS CO HUNTINGTON BEACH CALIF F/G 20/12

APPLICATION OF NONLINEAR CRYSTALS.(U)

JUL 79 C J KASTNER, J J GROSSMAN N00173-78-C-0161

UNCLASSIFIED MDC-G7887 NL

1 OF 1
ADA
077570

END
DATE
FILMED
1-80
DDC

14 MDC-G7887

B.S. 12

Report MDCG 7887

Contract No. N00173-78-C-0161 15

LEVEL II

AD A077570

9 FINAL REP[redacted]RT.

6 APPLICATION OF NONLINEAR CRYSTALS.

10 Carol J. Kastner M.S.

[redacted]

Jack J. Grossman Ph.D.

McDonnell Douglas Astronautics Co.

11 30 July [redacted]79

Huntington Beach, CA

389310

12 96

389310 gm

79 08 03 041

CONTENTS

Section 1
INTRODUCTION

This is the final report by McDonnell Douglas Astronautics Company (MDAC) of work conducted for the Naval Research Laboratories; Washington, D.C. under contract N00173-78-0161, titled "Application of Nonlinear Crystals." An oral presentation was made in Washington, D.C. on July 9, 1979 and the view foils used are included as Appendix A-I.

The body of this report is a narrative description of the July 9 presentation referencing Appendix A-I figures and comments. The outline used for the oral presentation is given on page A-2. Auxiliary theoretical material has been included in Appendixes A-II. The topics are keyed into this narrative in Section 1.1 and a summary of the report is given in Section 1.2.

1.1 Outline

A program overview including the work statement and contract history is given in Section 2. The body of the report starts in Section 3 where prior work on frequency conversion done primarily by the Russians is discussed briefly. In Section 4 a detailed description of experimental work carried out under this contract is divided into ten (10) subsections. In Section 4.1 the joint transform correlator work with HeNe is described. This is followed in 4.2 by a description of MDAC's newly acquired frequency conversion facilities. Section 4.3 is an analysis of the optical properties of NRL bit shifted photographic transparencies supplied for use on this project. A variety of experimental factors which contribute to upconversion efficiency, and resolution are described in Section 4.4 to 4.9 in the framework of upconversion/convolution operations. Last, in Section 4.10, an experimental test called the N-pattern test is described and illustrated for the evaluation of second harmonic generation (SHG) conditions as a function of temperature, angle, and SHG crystal translation and rotation. Next, upconversion and downconversion conditions for real time convolution and correlation operations are discussed in Section 5. Finally,

the conclusions on applications of nonlinear crystals for up- and downconversion are given in Section 6.1 and recommendations for further study are given in Section 6.2. Appendix A-I is the collection of view foils used for the NRL Program Review in Washington, D.C. Appendix A-II is a review of the basic theory behind frequency conversion, the correlation operator, and the correlation of optical data using nonlinear crystals.

1.2 Summary

Although personnel changes and experimental problems delayed the program, the main goals which were reached included establishing a diffraction limited, Nd:YAG facility for investigating nonlinear crystal interactions for applications to ODP, developed experimental procedures for optimizing ODP optical conversion efficiency, and defined the experimental conditions for performing two frequency correlation by both upconversion and downconversion. Equipment for three wavelength upconversion correlation/convolution are available for preliminary tests of this more complicated ODP process. Finally, we are ready to process the NRL bit shifted data to measure correlation accuracy and Space-Bandwidth Product (SBWP).

An N-pattern test was developed to determine optimum temperatures for using CD*A as a Fourier plane nonlinear crystal in up and downconversion. By measuring correlation peak widths using N-pattern test data the system resolution was found to be 11 ℓp/mm which was the diffraction limit of the lens. A 50 mm, f/4 lens is available to substitute in the 450 mm lens now in use. This will increase the resolution by a factor of 9 to 100 ℓp/mm.

Correlation and convolution can be interchanged by rotating real patterns. This is done by rotating 180° one of a pair of input patterns which is equivalent to complex conjugation in the Fourier plane domain. A test complex conjugate input pattern was prepared and is now ready to use for correlation by upconversion.

By using filters at the input and image planes, it is possible to identify the ODP terms and the different components contributing to signal and noise. In this way we were able to find the conditions for phase matching by temperature and angle tuning for downconversion using the N-pattern test.

Section 2
PROGRAM OVERVIEW

2.1 Statement of Work

A task breakout of topics to be covered is given on page A-5. In Task 1 correlation of two images was proposed using convolutional upconversion of Hermitian functions which in this special case is equivalent to the correlation. The Space-bandwidth product (SBWP) would then be measured from the correlation peak width at the output. This SBWP would then be compared, in Task II, with comparable SBWP values determined using an optical correlator and digital computer techniques. In Task III, the correlation which is generated as a bulk zero frequency field would be read out using a third frequency (color) HeNe. Task 4 was designed to demonstrate correlation of NRL codes in real time, find the bit shift accuracy by direct measurement and determine maximum bit density limitations. Last, Task 5 was to select crystals with large nonlinear coefficients, determine optimum pulse matching conditions, develop equations to characterize field angle, and then select, specify and purchase upconversion crystals for the experimental portion of this program.

2.2 Historical Summary

The program history is summarized on page A-6 and in Figure 1. Briefly, Peter Guilfoyle left the program in January, 1979 after the upconversion and laser crystals were ordered, and he and Carol Kastner completed the Joint Transform Correlator (JTC) laboratory work in January. C. Kastner then assembled the equipment and started upconversion experiments alone until May 1979 when J. Grossman joined the program. After correcting operational laser problems, some equipment modifications were implemented and the convolution work completed.

Section 3
PRIOR WORK ON CORRELATION AND CONVOLUTION

Eremeeva, et al. (Reference 1) published results in 1976 showing that optical convolution and correlation of two scenes, illuminated by two optical frequencies ω_1 and ω_2 respectively, could be accomplished using non-linear crystals. The convolution operation is obtained when the two frequencies are the sum ($\omega_1 + \omega_2$) frequency and the correlation operation is obtained when the two frequencies are the difference ($\omega_1 - \omega_2$) frequency. They published results (reproduced in Figure A-2), wherein they show the results of interaction of circular apertures illuminated by combinations of the fundamental color λ_1, the second harmonic λ_2 and the third harmonic λ_3. Inset a shows the three input plane hole symmetry patterns used. A companion background discussion is given in Sections 1 to 3, Appendix A-2.

Eremeeva calls case d auto-convolution because the same wavelength λ_1 is used to illuminate both holes which we distinguish as F and G, the Fourier transforms of scenes f and g at the input plane. Since the images are real, the Fourier tranforms also contain the complex conjugate functions F* and G*. Experimentally this is accomplished as shown schematically in Figure 3d. The laser 1 emits the fundamental λ_1 through a beam expander (in 1) and illuminates the object plane 4 through a filter 3 which passes only λ_1. The object plane 4 and a second harmonic generating crystal 6 are at conjugate focii of the Fourier transforming lens 5. Thus, the Fourier transforms (F + F*) and (G + G*) of the upper and lower object plane light distributions are multiplied by the non-linear crystal interaction to produce terms FF*, GG*, and FG* and F*G at $\tilde{\omega} = 0$ (the DC terms) and FF, GG, F*F*, G*G*, FG and F*G* at $\omega = 2\omega_1 = c/\lambda_2$ where c is the velocity of light (Reference 2). A second Fourier Transforming lens 5 images the convolutions and/or correlations (as the case may be) on image plane 7 through a second filter 3 which in, Figure 3d, passes only λ_2.

It is easy to identify the locations of the different terms. The interaction of the light through the upper aperture F with itself to produce the real convolution FF + F*F* at λ_2 appears at the lower position in the image plane. Similarly, the terms GG + G*G* appear at the upper image position. The cross-convolution FG + F*G* appears at a position halfway between the two.

The energy which is in the correlation terms goes into a local static deformation of the crystal at the Fourier plane which then relaxes at a rate controlled by potential energy dissipation by phonon emission. It was postulated that this field might be interrogated by a different frequency λ_i shown in Figure 3a. Taking into account the crystal distortion lifetime, the stress should be interrogated with a pulse at wavelength λ_i synchronized with the fourier-plane stress-generating pulse at λ_1. Since the ions in the crystal cannot respond to the electromagnetic generating field, a time delay will be required to permit the electronically stored DC field energy to transfer into lattice deformation before the DC field can be read out.

In correlation and convolutions of Figures 2b and c and 3b and c, the third harmonic λ_3 is also used. In this case a single upconversion crystal 2 is used to generate λ_1 and λ_2 at the input plane for convolution (case c) and crystals 2 and 3 are used to generate λ_1 and λ_3 at the input plane for correlation (case b).

The different combinations of input terms F_i and G_j which are connected with the λ_i and λ_j for correlation and convolution are summarized on the right hand side of Figure 2. The companion designations correlation, auto-correlation, convolution and auto-convolution are the Russian workers designation for the process of using different or the same wavelengths for downconversion (correlation) or upconversion (convolution).

A terminology problem becomes evident when we try to consider both wavelength and scene convolution/correlation. The Russians imply wavelength

and common usage implies pattern. This is shown on page A-11. There are essentially four cases shown in the two by two matrix. In what follows we propose to use the following rules. Correlation (convolution) and cross-correlation (cross-convolution) are synonomous. Auto-( ) refers to pattern convolution. Auto-λ- ( ) refers to down (up-) conversion using the same wavelength. Finally, auto-auto-λ- ( ) will be called A^2-( ) when a pattern is correlated (convolved) with itself by SHG.

Section 4
EXPERIMENTAL

4.1 Joint Transform Correlator (JTC)

As part of Task II (page A-5), 23 x 23 bit arrays both zero-shifted and 128 bit-shifted input patterns were correlated using the MDAC-JTC, Figure 4. These patterns and their output have been published (Reference 3) and discussed in detail there (See also Section 4, Appendix AII for some recent analytical work). These results will be compared at some future time with the equivalent real time data derived from optical processing with CD*A crystals.

4.2 Frequency Conversion Facilities

The Holobeam 5050Q Nd:YAG Laser was purchased based on lower cost, and quickest delivery. The Q-switched oscillator amplifier combination generates 65 mj per pulse with a 20 Hz repetition rate.

CD*A was found to be the best choice of crystals presently available for SHG. Three different length crystals, 5 mm, 10 mm and 20 mm, were purchased. Each having the same cross section (15 mm x 15 mm) cut perpendicularly to the optic axis for temperature tuning. A smaller crystal of RDP used for third harmonic generation (THG) is available for three frequency. It is too small and have convolution without excessive vignetting if used for down correlation in the Fourier plane.

The experimental equipment and setup are shown in the annotated Figures 5, 6, and 7.

4.3 NRL Transparencies

4.3.1 Resolution Tests with HeNe Laser

NRL sent transparencies of pseudo-random codes to MDAC to be used for measuring cross-correlation parameters using non-linear crystal interactions. As a first step, optical transmission and resolution tests were made using a HeNe laser with the CD*A crystal in and out of the Fourier plane. Some of these test results are shown in Figure 8. Two points are worth particular attention.

First, we find that the binary black and white imagery has a noise component where the black is not quite black Figure 8a, 10 sec exposure, and the white is not quite white, Figure 8d and e, 1/100 sec exposure. The existence of this "noise" component should be included in future S/N measurements of ideal resolution.

Second, multiple images appear, compare Figures 8a and 8b, when the CD*A crystal is placed in the Fourier plane. The most likely source is multiple reflection between the crystal surfaces and the input plane transparency. This one and others are important sources of noise which must be minimized or eliminated for optimum system operation (see Figures 11 and 12 following).

4.3.2 Convolution SHG and Transparency Rotation Tests

The A^2 convolutions (Types FF + F*F* and GG + G*G*) are found to be real because they are independent of transparency rotation (Figures 9a, b, and c). However, the wander of the faint pattern between the A^2-convolutions with respect to the center of rotation shows it is probably not the auto-2-convolution (FG + F*G*). This is verified by masking out alternately the F and G patterns, Figure 9d and e, noting the pattern remains. Although a part of the FG pattern wanders, the appearance of the edge cutoff in d and e suggests that the most likely source is the partial grey level transmission observed in Figure 8a, b, and c. Verification of these alternatives were not pursued.

Two points are worth emphasizing. First, the effects of non-uniform object plane illumination is apparent from the variation in the A^2-convolution intensity distribution with rotation. Secondly, a portion of the beam undergoes A^2-convolution (SHG) of the type FF, which reproduces the image. This shall be compared with auto-λ-convolution of the type F'F of different parts of the same pattern. This is another level of complexity to add to the classification matrix on page A-11.

4.4 Convolutions with Square Apertures

When the CD*A crystal is set at 102°, the optimum SHG temperature, and 5/16" input plane apertures are separated (center to center) by 1", Figure 10a, b and c, only A^2-convolutions are observed. However, when this separation is reduced to 1/2", the FG auto-λ-convolutions appear Figure 10d.

A number of additional features are worth noting. The A^2-convolution in Figure 10a shows a bright cross. However, the cross in d is dark. Even the multiple reflections at top have dark crosses. The main difference between the squares is the ones in d are larger then those in a in the ratio a:d :: 1:$\sqrt{2}$. A 90° rotation should normally produce no change for 4-fold symmetry. Yet, the lower squares in a have a 2-fold bright band symmetry along the horizontal diagonals. Finally the satellite reflections in c are found to have a pair of parallel dark bands.

The upper left A^2-convolution in Figure 10c is sufficiently dark than a square array of lines is visible with density 3 lp/mm. This places a lower limit on the resolution (see Section 4.10.3).

4.5 Use of Image Plane Filters - On Two Crystal Experiments

The configuration employed in this experimental arrangement is similar to that shown schematically in Figure 3c where both crystals 2 and 6 are CD*A set for 90° oriented SHG. In other words, in the relation $(\lambda_1 ; \lambda 2)(\lambda_3)$, $\lambda_2 \equiv \lambda_1$.

When a red filter is used in the input plane Figure 11c and d, we see both A^2- and auto-λ-convolutions. The A^2-convolutions are much lower in intensity as shown in c using low speed film. This is to be contrasted with the results already observed in Figure 9 where only A^2-convolutions were found.

Leaving out the red filter, Figure 11a, the green in the input passes through the system without change imaging the input circular holes in the photograph. By measuring the ratio of the intensities of the green light at the A^2 position with and without the red filter we can determine the A^2-convolution conversion efficiency. Similarly, the auto-λ-convolution efficiency can be found. This will be a valuable tool when evaluating system operation.

4.6 Internal Reflections, SHG and Noise

Internal reflections have already been discussed (Sections 4.3 and 4.4). The points of interest for Figure 12 and 13 are summarized on pages A-26, and A-28. Reflections are an important source of noise and will have to be minimized in system design. Possible solutions include:

a. Non-parallel crystal faces.

b. Index matching fluid.

c. Absorption filters in the SHG crystal Housing.

d. Anti-reflection coatings which transmit both the fundamental and second harmonic.

4.7 Convolution Non-linearity

The A^2-convolution process is basically a field squaring process so that areas in a scene which have twice the transmission will convolve to 4

times the intensity. This enhancement is graphically demonstrated in the convolutions shown in Figure 14.

4.8 Convolution Peak Intensity Ratios

The variations of the peak convolution intensity ratios is understood to depend on the angular extent of each input scene, the separation between them, temperature, the direction of the optic axis and the longitudinal position of the SHG crystal relative to the Fourier plane. Figure 15 is an example of CD*A angle effects. The effect of a 10°C rise in temperature is shown in Figure 16 where the central spot is a disappears in b and the A^2-convolutions become enhanced. Crystal translation and rotation are not as sensitive for 90" tuning as for angle phase matching. This is discussed in Section 4.10.4 in relation to Figure 22.

4.9 Crystal Damage

Moving the image plane 4.5 cm (∿10% of the focal length) does not appreciably change the A^2- and auto-convolution patterns Figure 17. However, it does affect high spatial frequency scattering associated with crystal damage from laser pulse energies which exceeded the damage threshold of CD*A at the Fourier plane. For example, the high frequency components associated with the upper circular aperture in Figure 17b disappears in c when the image plane is translated -4.5 cm towards the image plane lens. Simultaneously, scattering by damage appears at the lower right hand aperture. This demonstrates the insensitivity of convolutions (and correlations) to Fourier plane crystal damage which would be expected from visual inspection to degrade the image more than observed. It suggests that a crystal could be subjected to considerable damage without seriously modifying its effectiveness for up and down-conversion.

4.10 N-Test of CD*A

Second harmonic generation of laser radiation is maximized when the vector sum of the two upconverting photon wave vectors $\vec{k}_1$ equals the second harmonic wave vector $\vec{k}_2$. Since $k(\theta) = (2\pi/n(\theta)\ \lambda)\ \vec{S}(\theta)$, then for temperature tuned,

colinear SHG θ = 90° and the refractive indexes of the fundamental and second harmonic are equal. This is the usual A^2-correlation (convolution) doubling condition which for CD*A occurs at 102°C. When cross-correlations are to be performed, the input plane images are usually separated by at least the width of the scene. Then, the condition for phase matching becomes that the projections of the sum of the $\vec{k}_1$ vectors onto $\vec{k}_2$ shall be equal. In this case, the angle between the central rays of the two intersecting cones is about 5° to 6° and the phase mismatch is equivalent to a refractive index mismatch of .00274. This refractive index change can be obtained by lowering the temperature. However, as the temperature is lowered to achieve refractive index matching for the auto-λ-cross-correlation, the A^2-correlation index matching conditions are lost.

4.10.1 The N-Pattern Test

To determine rapidly the phase matching conditions as a function of temperature, an N was cut out of black paper 1-1/2" high and 1-3/8" wide. The width of the lines forming the verticlas and diagonal of the N was 0.1". An input plane N was illuminated by both 1.064 μm and 532 nm radiation (see Figure 3c, at 25°C). The results are shown in Figure 18a, b and c for different exposures. The green outline of the (backwards) N can be seen as well at wishbone shaped images which are the auto-λ-convolutions of the legs of the N with the diagonal. The joint of the wishbone is the 90° phase matched condition halfway between leg and diagonal and the arms of the wishbone are the equivalent angle matching conditions as the separation between the images change. When a red filter is used to absorb the green falling on the image plane, Figures 18d and e, the green light that remains in the 3 legs of the N are A^2-convolutions of each leg on itself.

4.10.2 Temperature and SHG

A series of N-tests were conducted for different Fourier plane crystal temperature, from 25°C to 100°C intervals. The results are shown in Figures 18, 19, 20 and 21 as the temperature is increased. The joint of

the wishbone moves towards the apexes of the N and at 100°C, which is close to "ideal" SHG temperature, the joint becomes coincident with the apex. The wishbone arms also come closer together and move towards the apex.

4.10.3 Effect of Exposure

Two effects of exposure on the film is seen. First the lines widen to a maximum limit and second additional segments of the legs of the N appear and second order intensity wishbones appear. In Figures 18, 19, and 20 additional wishbones appear in between the arms of the main wishbone, whereas in Figures 20 and 21, they appear on the side away from the apexes of the N. This shows that higher order terms in the polarization tensor product with the electric field are present and might contribute adversely to S/N.

If the low exposure frames in which the red filter was used are examined carefully, Figures 18d, 19c and 20d, a thin bright line (the central A^2-correlation peak) approximately 100 μm wide is found centered in the legs and diagonal of the N. This width is found to be in surprisingly good agreement with the expected resolution calculated from the system parameters $x/2\lambda f$ = (10 mm/2 x 1.06 x 10^{-3} x 400 =) 11.8 ℓp/mm. By using a shorter (100 mm) focal length Fourier plane crystal lens, it should be possible to increase the resolution to 40 ℓp/mm.

4.10.4 CD*A Angle and Translation Effects

When the CD*A crystal was translated vertically 3 mm off the optical axis, the convolution/correlation images disappear, Figure 22c. This sharp intensity decrease starting at 2.8 mm can be compared to crystal vignetting for the first 2 mm of motion Figure 22a and b. The effect of rotating the optical axis 0.8° is seen to be (the 90° temperature tuned wishbone joint) an intensity symmetry change in the wishbone joint from Figure 22b to d.

Section 5
DISCUSSION

The N-pattern test showed that as two input scenes are moved apart, the optimum temperature for 90° phase matching decreases. Examples of this are shown in Figure 23 where at 25°C using CD*A the A^2-convolutions are missing in all cases, and the auto-λ-convolution is found in e and f but absent in d. From Figure 18, the minimum distance for which cross-convolution should be observed is 2.6 mm ± 1 mm. Since the diagonal of the largest pattern, f, is only 21 mm, the absence of the A^2-convolution is not surprising. The cross convolution is also absent in d since the maximum width of the NRL data is 30 mm. Consequently, only 4 mm from the outside of the two patterns are used in the auto-λ-convolution.

The interaction area can be increased by increasing the temperature until the minimum distance for color conversion is 10 mm. However, this would cause A^2-convolutions since the diagonal is $\sqrt{2}$ cm. Suppression of the A^2-convolution, keeping the center to center pattern distance of 20 mm constant, is possible if the pattern width is decreased by $(\sqrt{2} - 1)$mm. Then if the DC field is read out using another wavelength laser, the A^2-correlations will not interfere.

When one of the input plane patterns is rotated 180° (forming the complex conjugate) the convolutions become equivalent to correlations. This was found to be true by examining the A^2-convolutions of the N-patterns. In them, there is a central white line about 100 μm wide which for the lens size used would give the expected diffraction pattern resolution limit of 11 ℓp/mm. Therefore, improved resolution is possible using a lens with a shorter focal length. A factor of 9 improvement in resolution 18 is theoretically possible by using a 50 mm lens at f = 1.6.

Using upconversion there are two ways to obtain correlations. These are:

a. Temperature tune - one central green pattern - FG* + F*G

b. Angle tune - two green patterns - FG* and F*G

This latter case is one in which the arms of the wishbone pattern are used (resolution of narrower angle tuning permitting) one being FG* and the others F*G. In the former case the 1st order diffraction pattern would be used to separate FG* and F*G from the central image. In this case the suppression of the A^2-correlations discussed above is mandatory.

Downconversion interchanges the roles of correlation and convolution. Normal patterns (both oriented the same direction) produce correlation and rotated patterns produce convolution. When only two wavelengths are used (the fundamental, λ_1, and second harmonic, $\lambda 2$) with normal patterns, correlations are produced $(\lambda_1, \lambda_1) \rightarrow$ (DC)

c. Temperature tune - DC pattern

d. Angle tune - DC pattern

The readout is affected by a second laser, at any convenient wavelength, which is synchronized with and delayed in time from the IR laser drive pulse to allow maximal transfer of stored slectron energy into a stress field which scatters the readout light pulse.

Another correlation process is assymetric downconversion using two or three wavelengths. These are:

e. $(\lambda_1, \lambda_2) \rightarrow (\lambda_2^1, \lambda_1)$ T 4

f. $(\lambda_1, \lambda_3) \rightarrow (\lambda_2^1, \lambda_2)$

Energy and momentum conservation suggest that:

g. $(\lambda_1, \lambda_2) \rightarrow (\lambda_2^1, \lambda_1^1)$	Tuning Mode Temp.	λ_1	λ_2^1	λ_2	λ_1^1
h. $(\lambda_1, \lambda_3) \rightarrow (2\ \lambda 2)$	4 T	λ_1		λ_2	λ_3
or	4	λ_3	λ_2		

In the diagrams to the right of e and f the dotted circles are the input plane wavelengths and positions at the crossed circles represent the image plane correlations. In e the input plane dots and crosses can be interchanged as the alternate version. In f the two input/output plane configurations are shown. The difference between temperature and tuning is that the λ_2 s are at positions 1/3 and 2/3 the λ_1 λ_3 separation for temperature tuning but are multiplied by constants (k) and (1-k) respectively for angle tuning. Asymmetrical conversion $(\lambda_1, \lambda_2) \rightarrow ({}_3)$ which wasn't discussed above is not the inverse of f. Similarly, $(\lambda_2, \lambda_3) \rightarrow (\lambda_1, 2\lambda_2)$ are more complex processes which will not be discussed here.

Section 6

CONCLUSIONS AND RECOMMENDATION

6.1 Conclusions

In this study we have demonstrated that upconversion correlations are being controlled by the diffraction limited resolution of the lens, 11 ℓp/mm. Since the basic equipment is working well, the input plane Fourier transform lens should be replaced using a high quality 50mm lens with an f/4 aperture or wider. The equipment will be ready then to find the maximum resolution and space bandwidth product by a variety of correlation methods. In order of simplicity for integration into real system applications. The correlation methods are:

1. Upconversion - rotated input format
   - 1.1 $(\lambda_1, \lambda_1) \rightarrow (\lambda_2)$
   - 1.2 $(\lambda_1, \lambda_2) \rightarrow (\lambda_3)$
2. Down Conversion - normal input format
   - 2.1 $(\lambda_1, \lambda_2) \rightarrow (\lambda_1', \lambda_2')$
   - 2.2 $(\lambda_1, \lambda_3) \rightarrow (2\lambda_2)$
   - 2.3 $(\lambda_1, \lambda_1) \rightarrow (DC)$ Laser Readout of DC Field

Joint transform correlator work has shown that prons and liquid crystal devices have resolutions up to 20 ℓp/mm. With 1 inch aperture this would correspond to a SBWP = $(20 \times 25)^2$. To equal or exceed this value the nonlinear crystal would require an input resolution of 50 ℓp/mm and 1 cm aperture. The tests to date suggest this is realistic.

The N-Pattern test is a very useful experimental tool which can be developed for optimizing system operation.

6.2 Recommendation

6.2.1 Finish Single Frequency Upconversion Experiment with Complex Conjugates

6.2.1.1 Use NRL Bit Shifted Data

6.2.1.2 Experimental/Theoretical Study: 2 Frequencies Up/Down Conversions

Both temperature and angle tuning (modified N-test).
Resolution vs. angular width of each image.
Resolution vs. intersection angle 2 images.

6.2.2 Additional Topics to Consider

6.2.2.1 Ruby Laser Readout of "zero Freq" Correlation Field

6.2.2.2 Two Crystal Downconversion Correlation: Image Scaling

6.2.2.3 For Completeness: Reproduce Russian 3 Crystal Up/Down Conversion

REFERENCES

1. Eremeeva, R. A., V. A. Kudryashov, I. N. Mataveev, T. G. Usecheva, and A. I. Chek Menev, "Convolution and Correlation of Optical Signals by Nonlinear-Optics Techniques," Sov. J. Quant. Electron., 5, No. 12, 1429-1430 (1976).

2. Guilfoyle, P. S., "Fourier Transform Plane Superposition Multiplier: Theory, Experimental Results, and Discussion."

3. Guilfoyle, P. S. and C. J. Kastner, "Optical Processing of Spread Spectrum Signals," Interim. Opt. Comput. Conf. 5-8 September 1978. (To be published in conference proceedings.)

MDAC CONTRACT REVIEW

OF

APPLICATION OF NONLINEAR CRYSTALS

NAVAL RESEARCH LABORATORY

JULY 9, 1979

OUTLINE

- SUMMARY
- PROGRAM TIMELINE - REVIEW
- RUSSIAN EXPERIMENTAL RESULTS
- EXPERIMENTAL EQUIPMENT
- RESULTS
- CONCLUSIONS
- RECOMMENDATIONS

SUMMARY

BAD NEWS:

- PERSONNEL CHANGES
- EXPERIMENTAL PROBLEMS

GOOD NEWS:

- DEMONSTRATED CONVOLUTION
- READY TO UPCONVERT USING COMPLEX CONJUGATES.
  IN THIS CASE CONVOLUTION AND CORRELATION ARE EQUIVALENT.
- DEVISED N-PATTERN/FILTER TEST PROCEDURE

  STUDIED ANGLE TUNING UP- AND DOWN-CONVERSION

  TEMPERATURE TUNING
- DEMONSTRATED CONDITIONS FOR DOWN CONVERSION CORRELATION
  USING N-PATTERN TEST

THIS PAGE INTENTIONALLY LEFT BLANK

JUNE 1978 STATEMENT OF WORK

TASK 1. SUPERPOSITION MULTIPLIER PARAMETERIZATION

- SINCE PSEUDO RANDOM SEQUENCES ARE HERMITIAN, PROPOSED TO USE UPCONVERSION SET-UP.
- SPACE-BANDWIDTH PRODUCT DETERMINED BY VARYING BIT DENSITY AT INPUT AND MEASURING CORRELATION WIDTH AT OUTPUT.

TASK 2. OPTICAL/DIGITAL COMPARISON

- PROCESS MAXIMAL LENGTH 511 BIT SEQUENCE BINARY DATA USING NONLINEAR CRYSTALS, A FILMED BASED OPTICAL CORRELATOR AND DIGITAL TECHNIQUES.

TASK 3. THREE-FREQUENCY INTERACTION

- OBTAIN CORRELATION (RATHER THAN CONVOLUTION) DATA BY USING BEAM OF A THIRD COLOR TO READ OUT ZERO-FREQUENCY FIELD.

TASK 4. CORRELATION OF NRL CODES

- DETERMINE BIT-SHIFT ACCURACY BY DIRECT MEASUREMENT.
- DEMONSTRATE REAL-TIME OPERATION.
- FIND BIT DENSITY LIMITATION.

TASK 5. CRYSTAL RECOMMENDATIONS

- SELECT CRYSTAL WITH LARGE NONLINEAR COEFFICIENTS.
- DETERMINE OPTIMUM PHASE MATCHING ANGLES FOR VARIOUS CRYSTAL TYPES.
- DEVELOP EQUATIONS TO CHARACTERIZE FIELD ANGLE.

HISTORICAL SUMMARY

- UNSOLICITED PROPOSAL SENT JANUARY 1978.
- PETER GUILFOYLE TO MANAGE OPTICAL PROCESSOR EXPERIMENTAL WORK.
- PATRICK KWOK: RESPONSIBLE FOR NONLINEAR CRYSTAL STUDY. TO DEVELOP EQUATIONS TO EVALUATE FIELD ANGLE, TEMPERATURE EFFECTS AND PHASE MATCHING CONDITIONS.
- LASER, CRYSTALS PROCURED, DELIVERED AND ASSEMBLED BY JANUARY 1979.
- GUILFOYLE AND KWOK TRANSFERRED OFF OF PROJECT BY JANUARY 1979.
- CONVOLUTION CONFIGURATION ASSEMBLED. NRL AND SIMPLE IMAGERY STUDIED THRU APRIL 1979.
- LASER REALIGNED AND CHECKED IN MAY.
- PRESENT TIME: REASSEMBLING SETUP TO DO CORRELATIONS BY UPCONVERSION OF COMPLEX CONJUGATES, RUBY READOUT OF DC FIELD CORRELATION, TWO FREQUENCY DOWN-CONVERSION AND THREE FREQUENCY DOWN-CONVERSION.

FIGURE 1

APPLICATION OF NON-LINEAR CRYSTALS PROGRAM SUMMARY

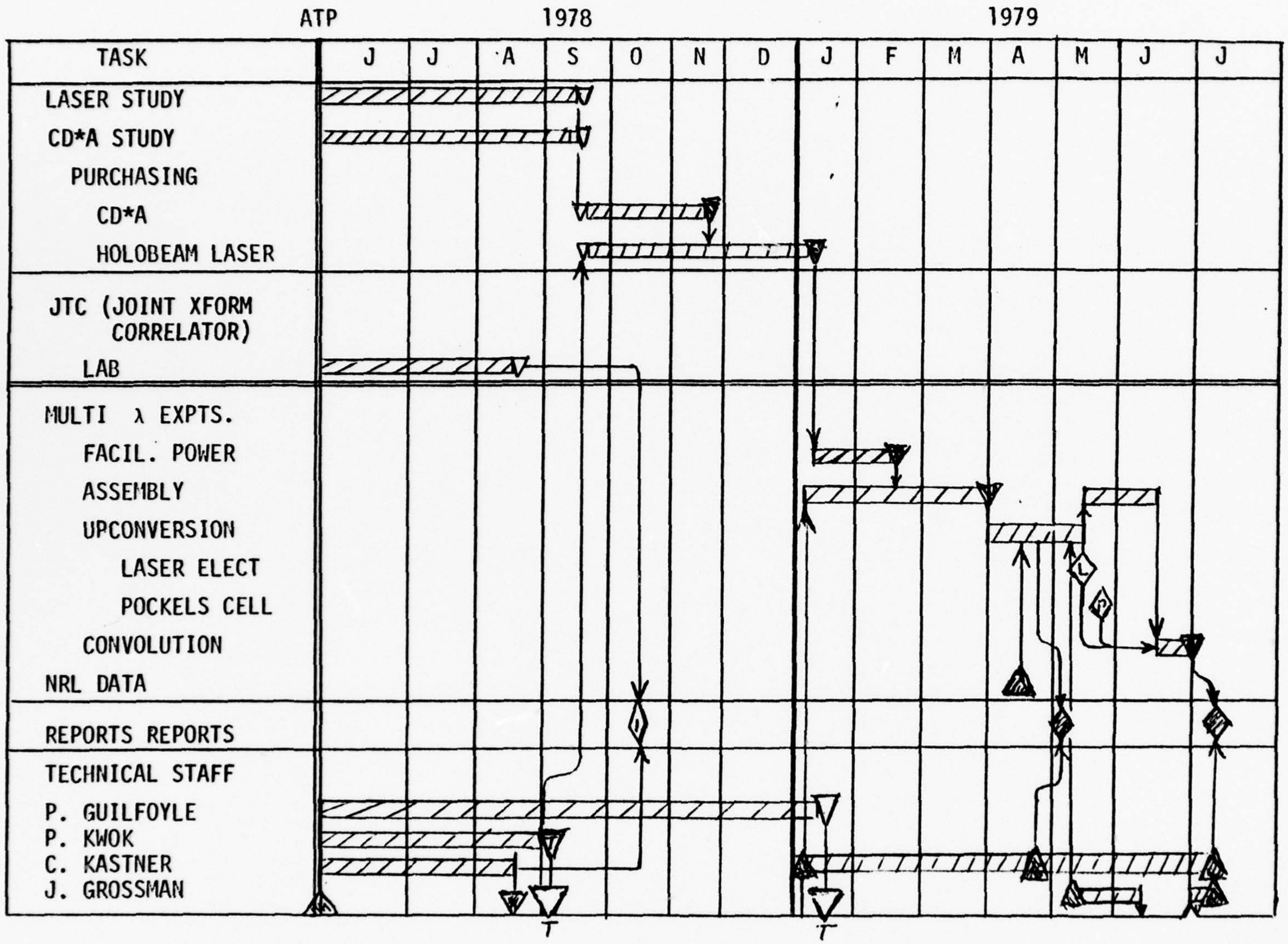

FIGURE 2

STANDARD PATTERNS OF CORRELATIONS AND CONVOLUTIONS USING NONLINEAR CRYSTAL INTERACTIONS

CONVOLUTION

$$u_+ = \sigma_+ u_{10} u_{20} e^{j(\omega_1+\omega_2)t}$$

$$U_+ = U_{10}\, U_{20}$$

CORRELATION

$$u_- = \sigma_- u_{10} u^*_{20} e^{j(\omega_1-\omega)t}$$

$$U_- = U_{10} U^*_{20}$$

REF: R.A. Eremeeva, et al., "Convolution and correlation of optical signals by nonlinear optics techniques," Sov. J. Quant. Tech., 5, No. 12, 1429-1430 (1976).

a

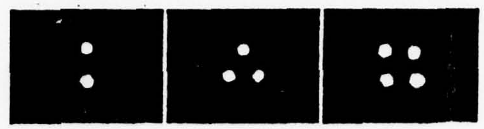

AUTOCORRELATION

$(\lambda_1;\lambda_1) \rightarrow (DC)$

$\begin{Bmatrix} F \\ F^* \end{Bmatrix} ; \begin{Bmatrix} G \\ G^* \end{Bmatrix}$ $(FG^* + F^*G)$ FF^* GG^*

b

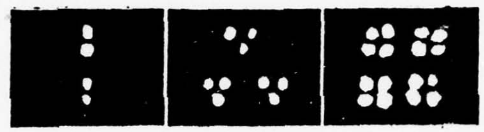

CORRELATION

$(\lambda_1;\lambda_3) \rightarrow (\lambda_2)$

$\begin{Bmatrix} F \\ F^* \end{Bmatrix} ; \begin{Bmatrix} G \\ G^* \end{Bmatrix} \rightarrow$ FG^* ; F^*G FF^* GG^*

c

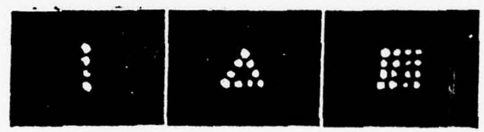

CONVOLUTION

$(\lambda_1;\lambda_2) \rightarrow (\lambda_3)$

$\begin{Bmatrix} F \\ F^* \end{Bmatrix} ; \begin{Bmatrix} G \\ G^* \end{Bmatrix} \rightarrow$ FG ; F^*G^* $FF + F^*F^*$ $GG + G^*G^*$

d

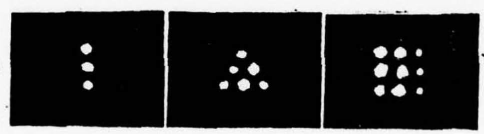

AUTOCONVOLUTION

$(\lambda_1;\lambda_1) \rightarrow (\lambda_2)$

$\begin{Bmatrix} F \\ F^* \end{Bmatrix} ; \begin{Bmatrix} G \\ G^* \end{Bmatrix} \rightarrow$ $FG + F^*G^*$ $FF + F^*F^*$ $GG + G^*G^*$

FIGURE 3

SCHEMATIC DIAGRAM OF CONVOLUTION AND CORRELATION USING NONLINEAR OPTICS

AUTO-λ-CONVOLUTION

$(\lambda_1,\lambda_1) \longrightarrow (\lambda_2)$

CONVOLUTION

$(\lambda_1,\lambda_2) \longrightarrow (\lambda_3)$

CORRELATION

$(\lambda_1,\lambda_3) \longrightarrow (\lambda_2)$

AUTO-λ-CORRELATION

$(\lambda_1,\lambda_1) \longrightarrow \infty \ (\lambda(DC) = \infty)$

d.

c.

b.

a.

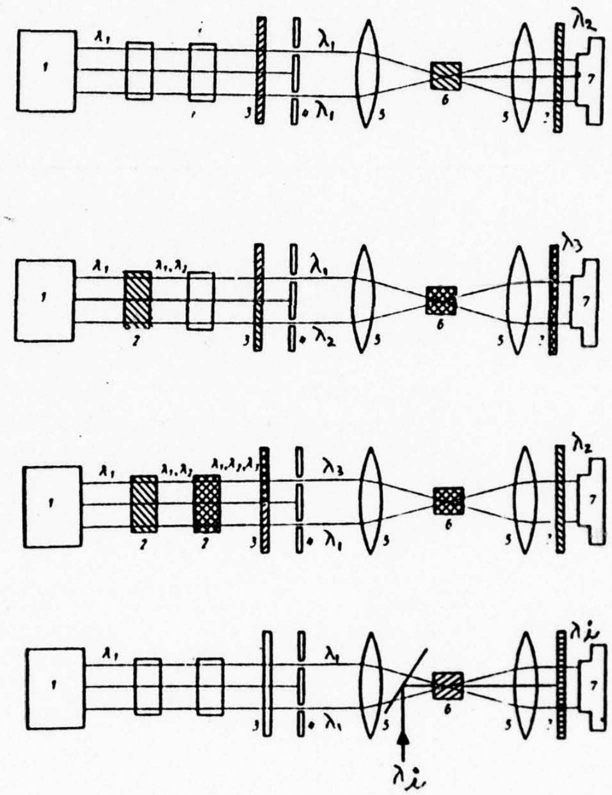

CONVOLUTION DEFINITIONS

RUSSIAN DEFINITIONS BASED ON λs

- Convolution: $(\lambda_1, \lambda_2) \longrightarrow (\lambda_3)$
- Auto-convolution: $(\lambda_1, \lambda_1) \longrightarrow (\lambda_2)$ (SHG)

COMMON USAGE BASED ON PATTERNS f AND g.

- Convolution: $f \circledast g$
- Auto-convolution: $f \circledast f$; $g \circledast g$

POSSIBLE PREFIX-MATRIX SOLUTION

- Rows based on f*g and f*f
- Columns based on λs
- Select prefix given by row column intersection.

	(λ_1, λ_2)	(λ_1, λ_1)
f*g	(None)	auto-λ
f*f	auto	A^2

FILM-BASED CORRELATION OF PSEUDO-RANDOM CODES

ZERO SHIFT

- CORRELATION PEAK 25 db ABOVE NOISE PEAK 200 μm WIDE AT ZEROS, USING 100 μm/BIT SEQUENCES
- ONE PEAKS ON EITHER SIDE OF DC TERM

BIT SHIFT

- 128 BITS DELAYED, USING WRAPAROUND FORMAT
- EACH CORRELATION REGION CONTAINS 4 PEAKS ABOVE NOISE. EACH CORRESPONDS TO FRACTION OF ZERO SHIFT DATA

FIGURE 4

FILM-BASED CORRELATION OF PSEUDO-RANDOM CODES

INPUT

23 X 23 BIT ARRAY GENERATED USING SHIFT REGISTER SEQUENCE OF LENGTH 511.

ZERO-SHIFT INPUT

128 BIT-SHIFT

OUTPUT

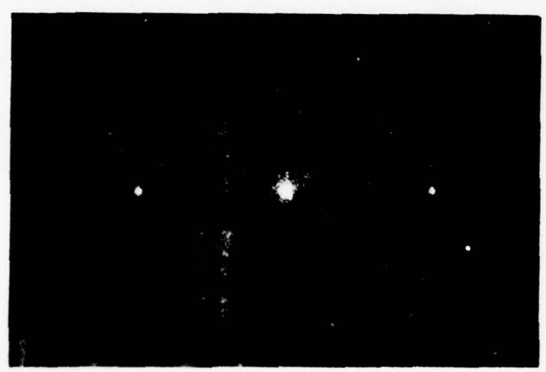

ZERO-SHIFT

BIT-SHIFT SHOWING CORRELATION PEAKS FOR SECTIONS MATCHED TO REFERENCE.

FACILITIES

HOLOBEAM 5050Q Nd:YAG LASER

- LOWER COST AND QUICKEST AVAILABILITY OF SYSTEMS CONSIDERED.
- 65 mj PER PULSE WITH 20 HZ REPETITION RATE.
- CAN BE MODE-LOCKED IF FUTURE REQUIREMENTS DEMAND HIGHER PULSE REPETITION FREQUENCIES.

CD*A NONLINEAR CRYSTALS

- HIGHEST OVERALL SECOND HARMONIC GENERATION EFFICIENCY.
- OPTICALLY TRANSPARENT AT 1.06μ AND .53μ.
- 90° PHASE MATCHING ELIMINATES BEAM WALK-OFF.
- INHERENTLY LARGE ANGULAR ACCEPTANCE.
- CD*A CHOSEN OVER CDA SINCE LESS CRITICAL TEMPERATURE TOLERANCE.

FIGURE 5

Nd:YAG LASER AND INPUT OPTICS FOR UP/DOWN CONVERSION

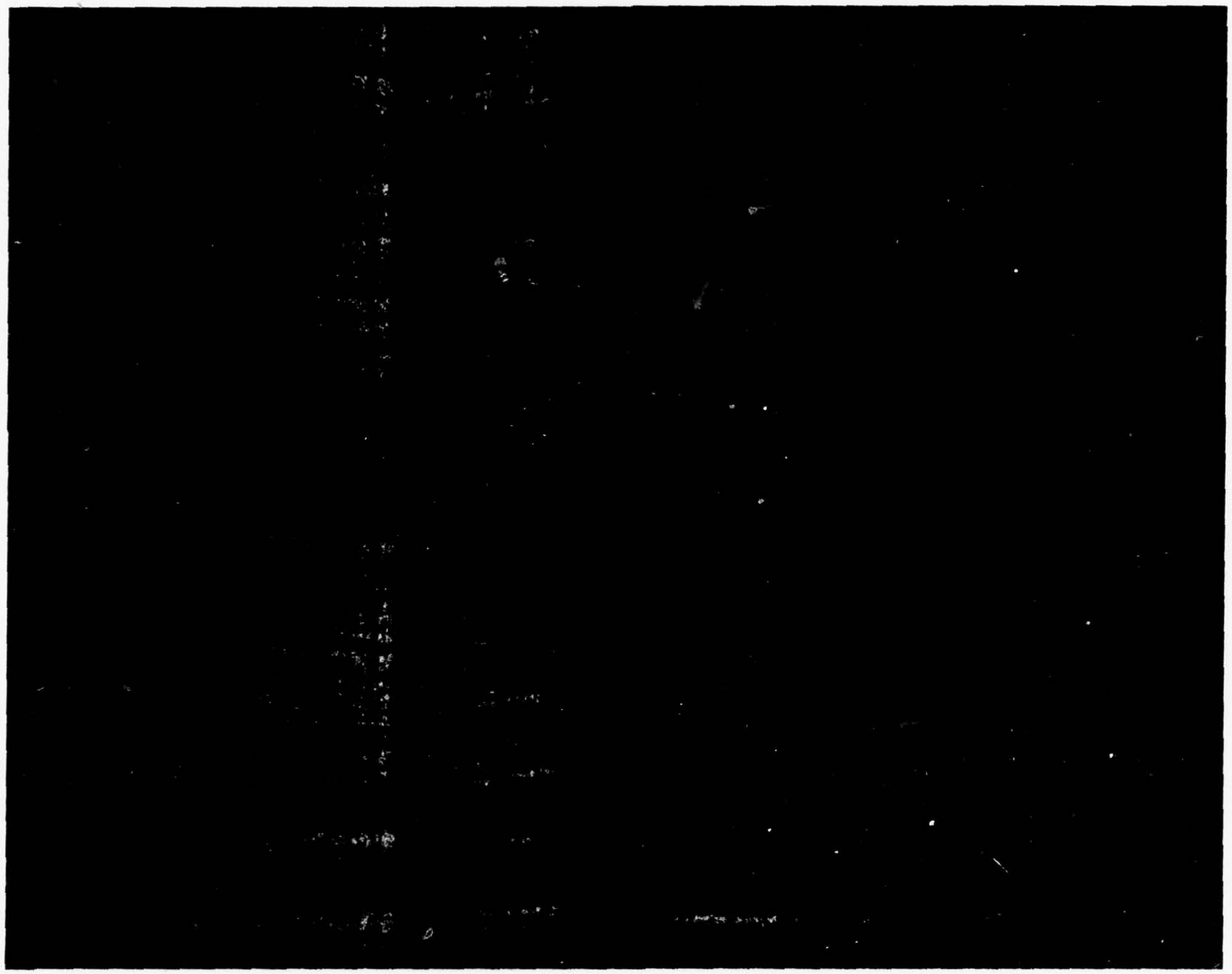

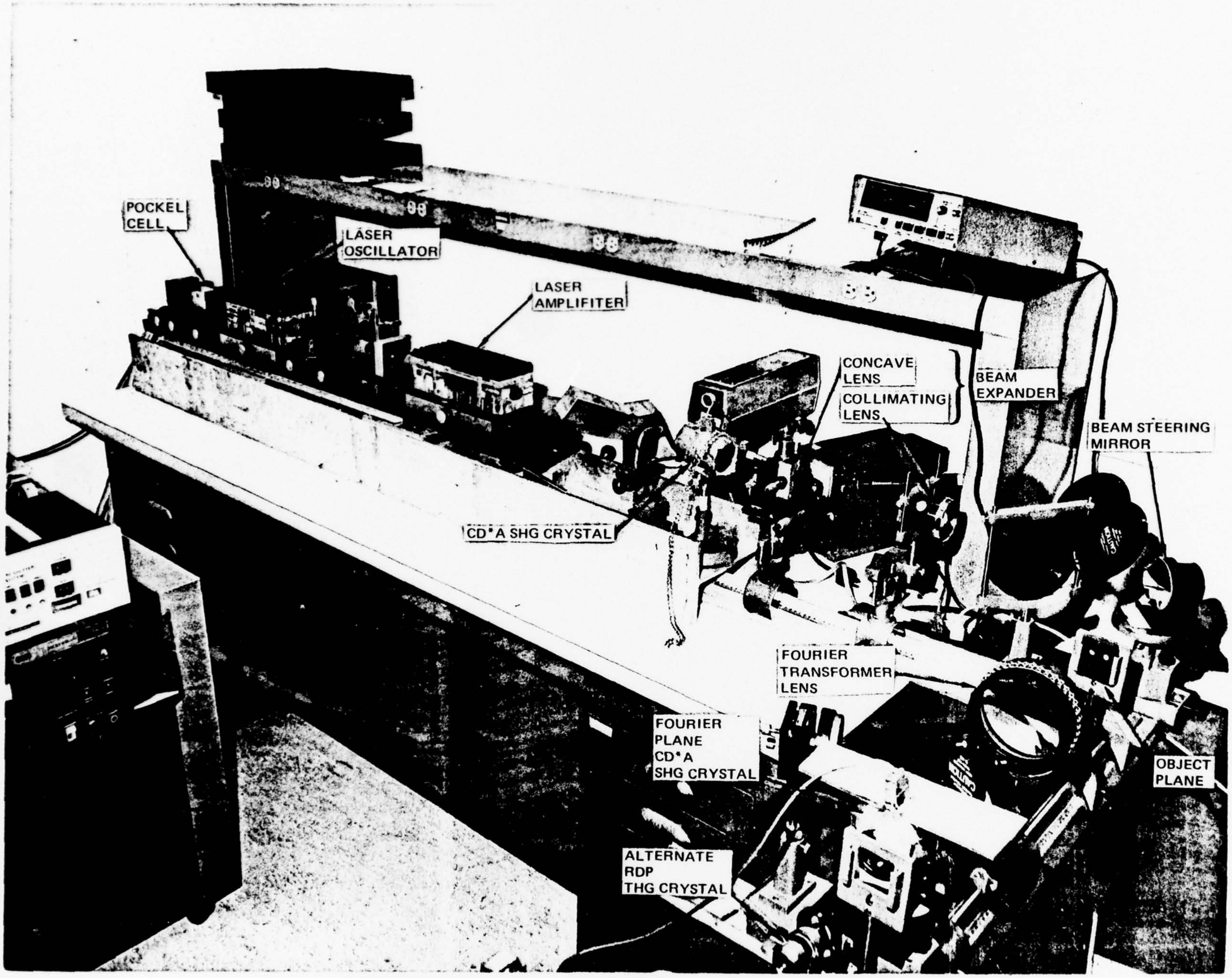
POCKEL CELL
LASER OSCILLATOR
LASER AMPLIFITER
CONCAVE LENS
COLLIMATING LENS
BEAM EXPANDER
BEAM STEERING MIRROR
CD*A SHG CRYSTAL
FOURIER TRANSFORMER LENS
FOURIER PLANE CD*A SHG CRYSTAL
OBJECT PLANE
ALTERNATE RDP THG CRYSTAL

FIGURE 6

INPUT PLANE AND BEAM STEERING OPTICS

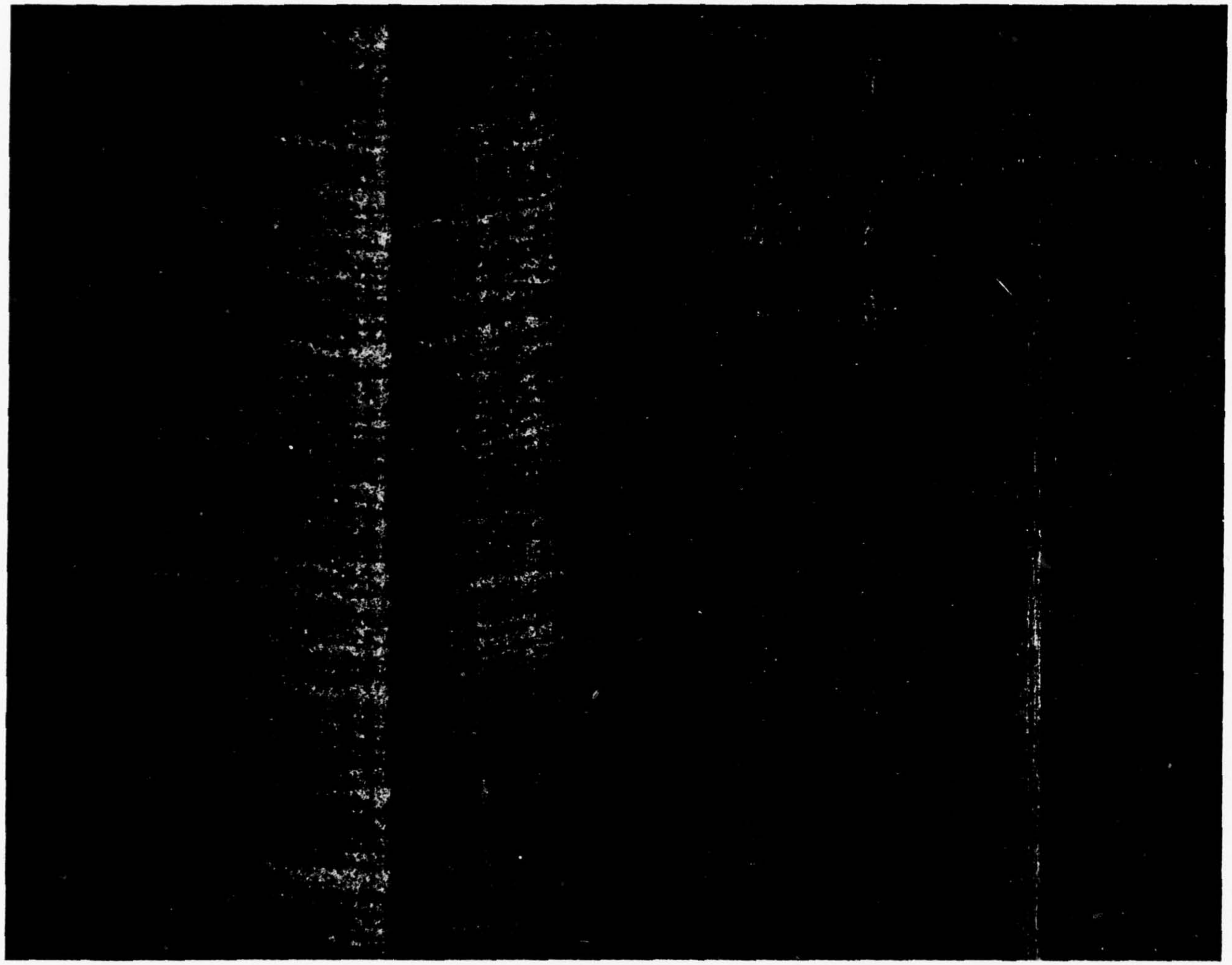

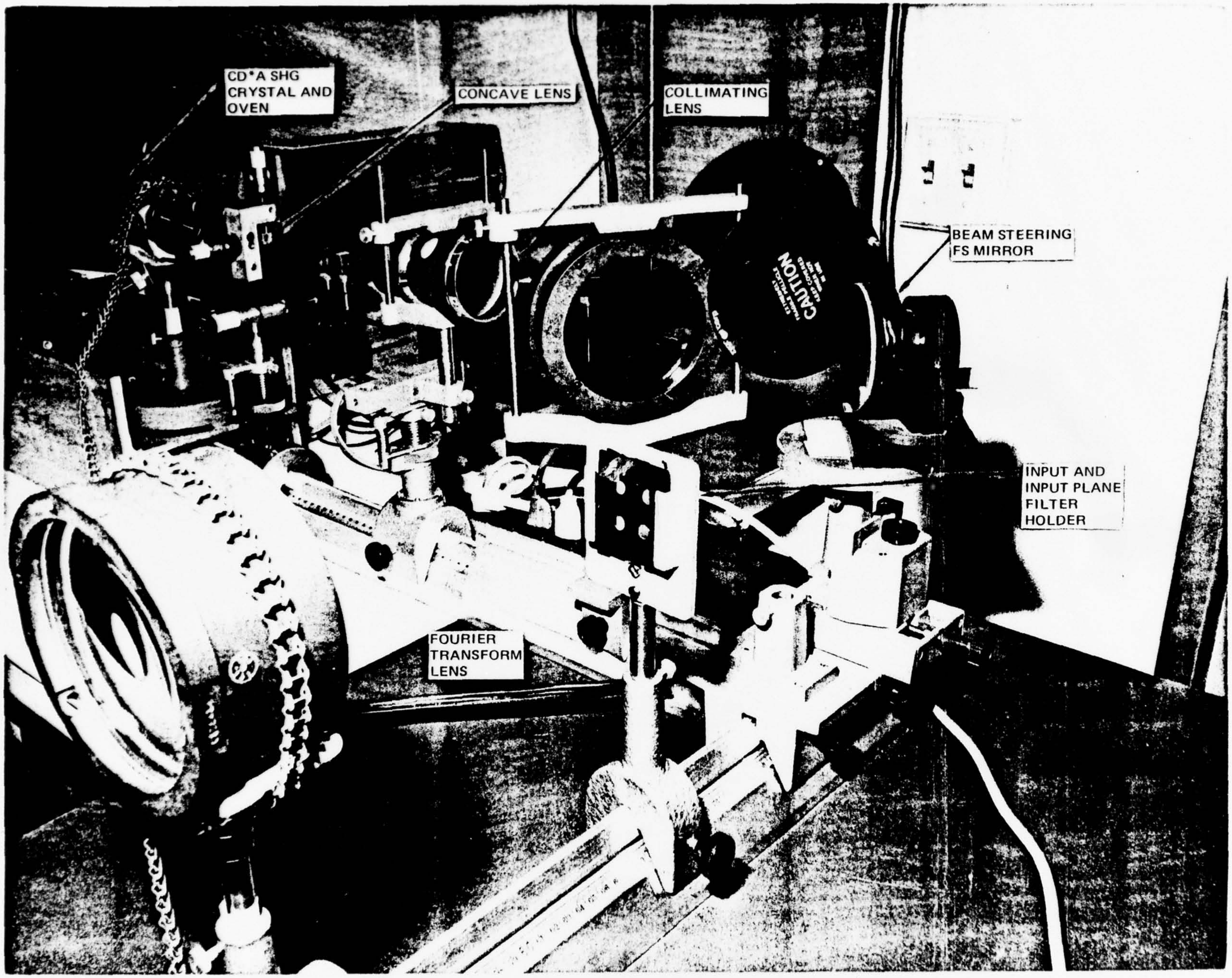

CD*A SHG CRYSTAL AND OVEN
CONCAVE LENS
COLLIMATING LENS
BEAM STEERING FS MIRROR
INPUT AND INPUT PLANE FILTER HOLDER
FOURIER TRANSFORM LENS
CAUTION

FIGURE 7

EXPERIMENTAL FREQUENCY COVERSION EQUIPMENT

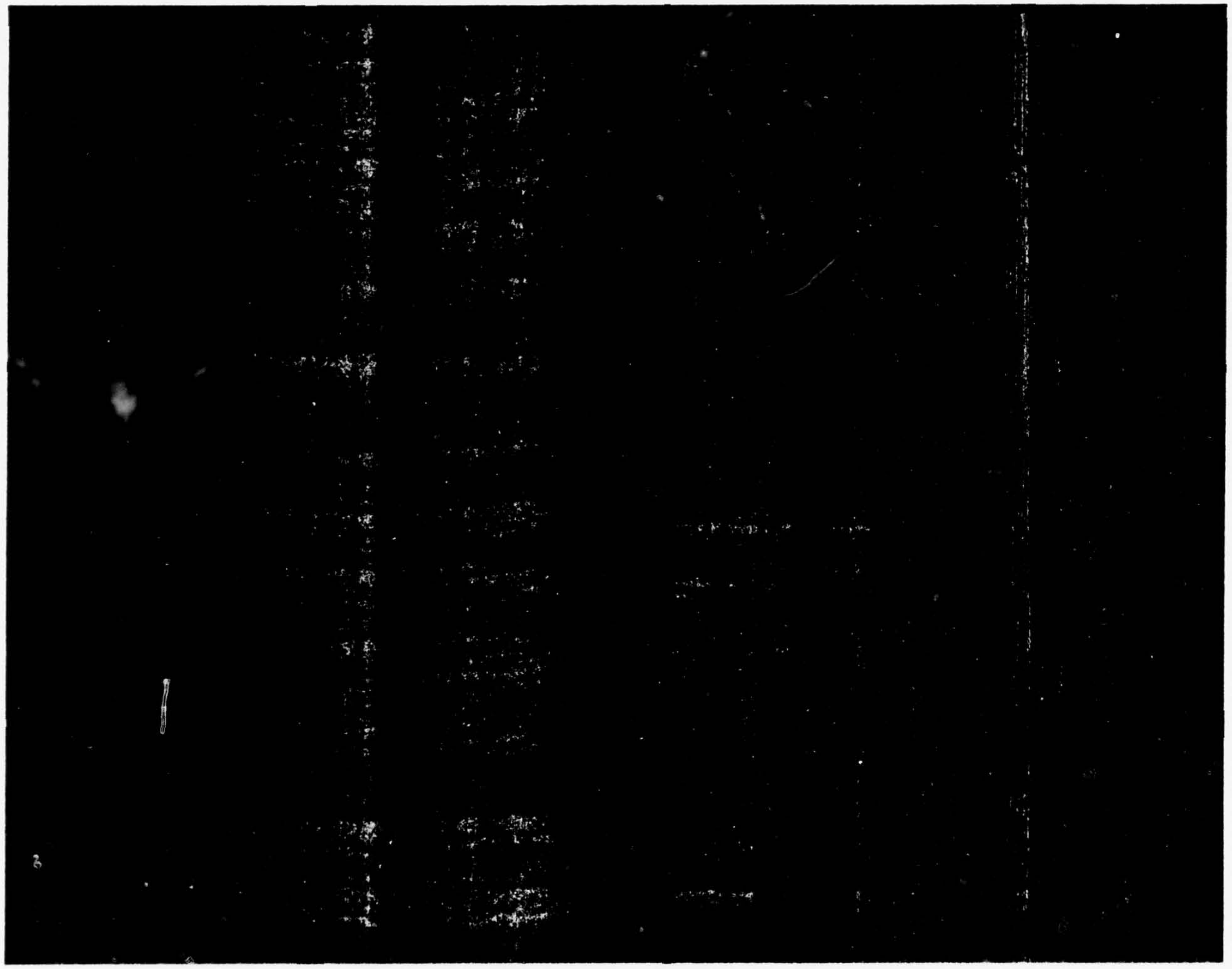

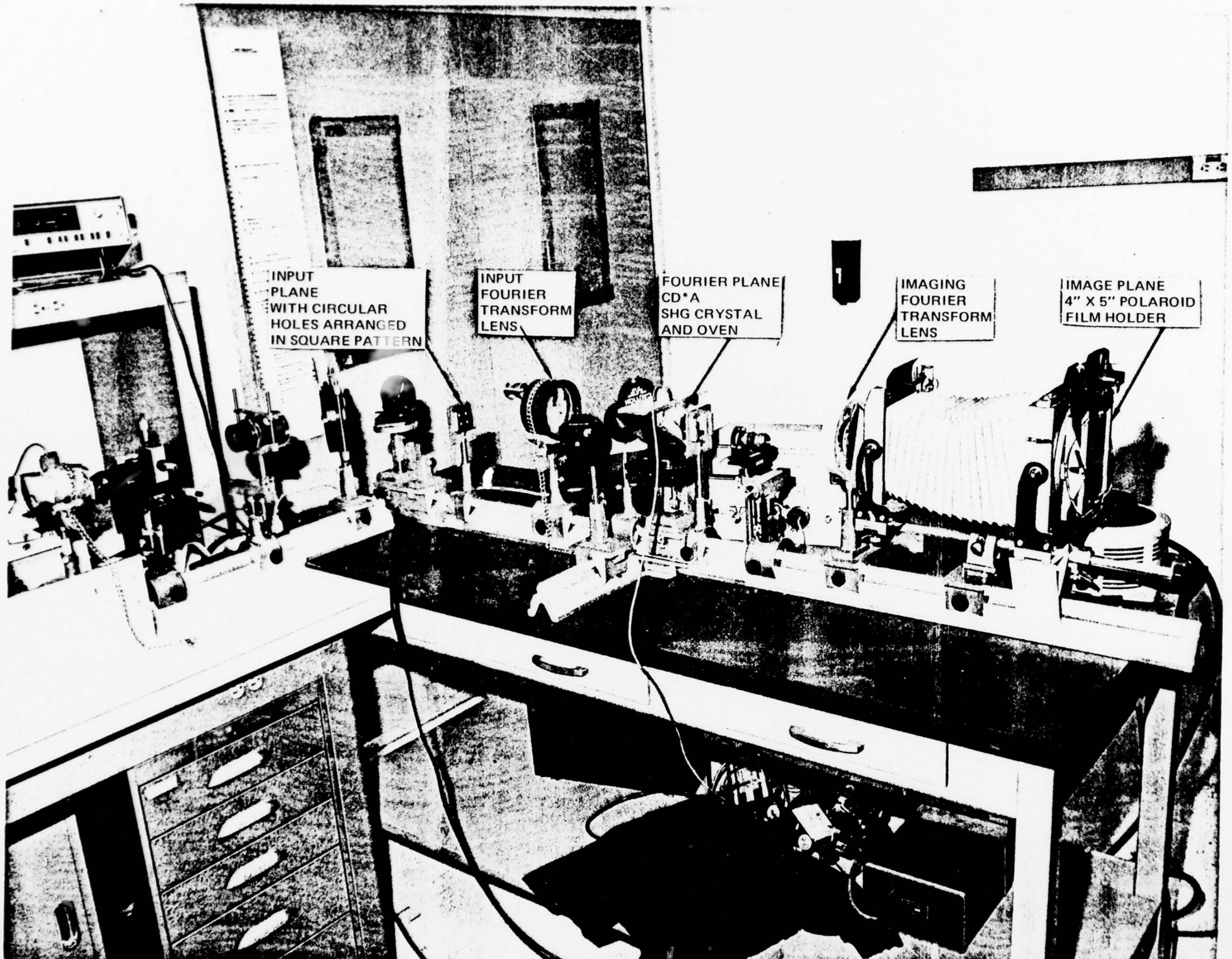
INPUT PLANE WITH CIRCULAR HOLES ARRANGED IN SQUARE PATTERN
INPUT FOURIER TRANSFORM LENS
FOURIER PLANE CD*A SHG CRYSTAL AND OVEN
IMAGING FOURIER TRANSFORM LENS
IMAGE PLANE 4" X 5" POLAROID FILM HOLDER

RESOLUTION TESTS USING NRL
35MM TRANSPARENCIES OF BIT SHIFTED CODES

CAPTION:

b taken with CD*A Crystal in Fourier Plane.

a, c, d and e without Fourier Plane Crystal.

Exposure time given using HeNe alignment laser 632.8 nm.

COMMENTS:

BIT SHIFT PATTERN EXPOSURE SPECKLE NOISE

- Background Black is Dark Grey (a and c)
- Bit Pattern White is Light Grey (d and e)

CD*A FOURIER PLANE CRYSTAL LINEAR EFFECTS ON 632.8 nm.

- Multiple Images in b Due Reflections
- Ring Interference Pattern

FIGURE 8

RESOLUTION TESTS USING NRL 35 MM TRANSPARENCIES OF BIT SHIFTED CODES

WITH CD*A CRYSTAL

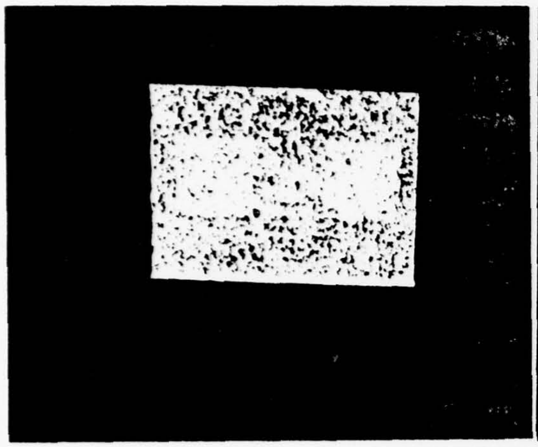

a. 10 sec.

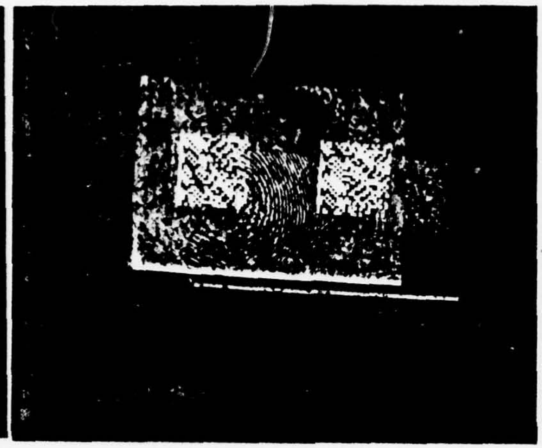

b. 10 sec.

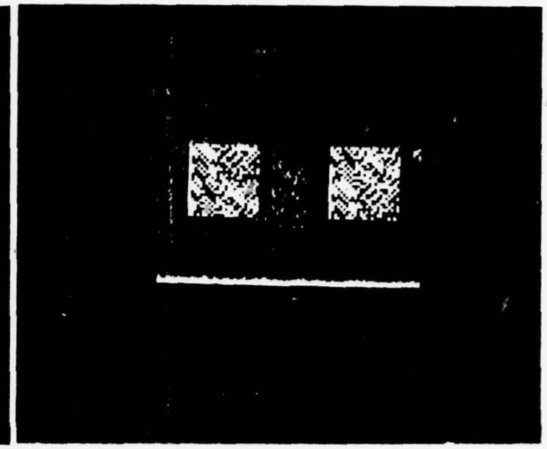

c. 2 sec.

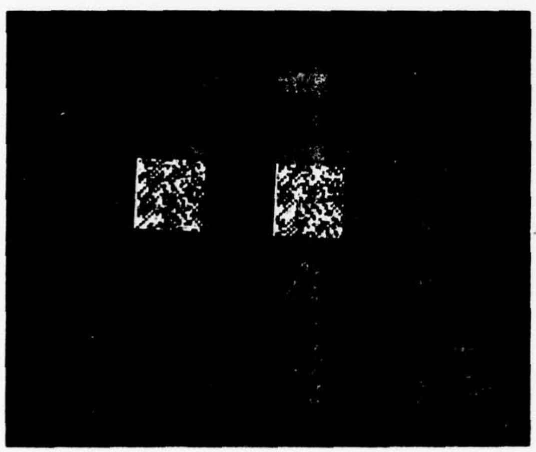

d. 1/100 sec.

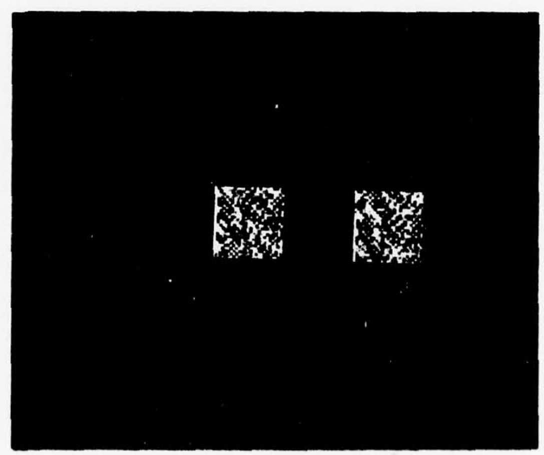

e. 1/100 sec.

ROTATION AND MASKING OF NRL TRANSPARENCY CONVOLUTION TESTS

CAPTION:

a. 90° clockwise rotation of b.

c. 90° counterclockwise rotation of b.

b and d. right image masked.

b and e. left image masked.

COMMENTS:

BIT PATTERN ROTATION a, b and e.

- A^2-convolutions are real.
- Main changes attributable to non-uniform illumination of object plane.
- Pattern in auto-λ-convolution area rotates with object plane and in addition translates.

ALTERNATE MASKING OF RIGHT AND LEFT d AND e.

- Has no effect on A^2-convolutions.
- Pattern remains in auto-λ-convolution area.

CONCLUDE NO AUTO-λ-CONVOLUTION SIGNAL PRESENT

FIGURE 9

ROTATION AND MASKING OF NRL TRANSPARENCY: CONVOLUTION TESTS

a.

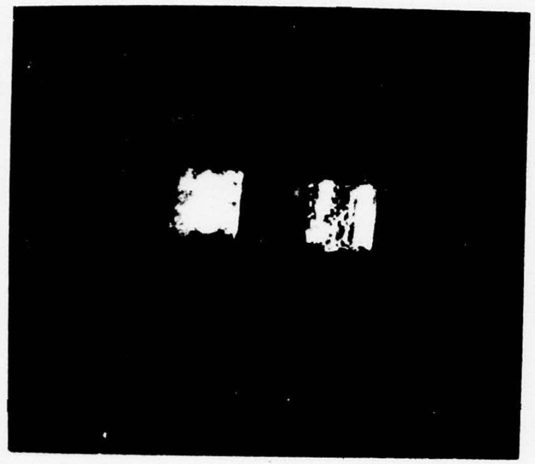

b.

c.

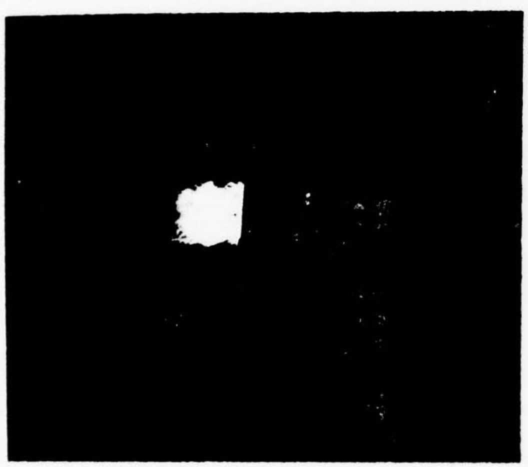

d.

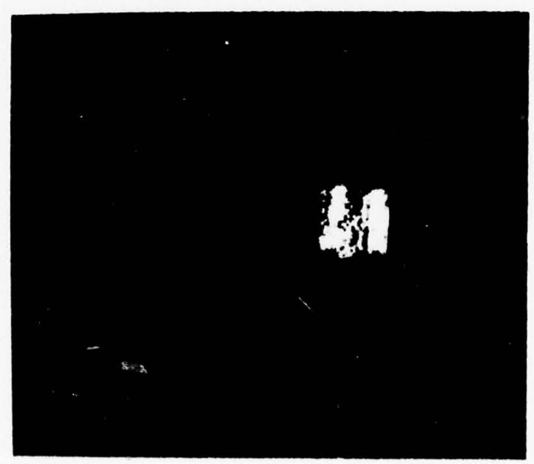

e.

CONVOLUTIONS WITH SQUARE APERTURES

CAPTION:

a. and b. square aperture diagonals vertical and horizontal.

c. 4 hole normal square pattern.

d. 5 square and 1 rectangle pattern with convolutions.

a and c. Type 52 Polaroid.

b and d. Type 57 Polaroid high speed film.

COMMENTS:

Spacings of squares too large for auto-convolutions except in d.

Crosslike A^2-convolutions in a and d are negatives of each other.

AUTO-λ-CONVOLUTIONS IN d: SERIES OF VERTICAL LINES

- Vertical line structure continued in upper left pair of A^2-convolutions.
- Horizontal dark line in auto-λ-convolutions.

SATELLITE A^2-CONVOLUTIONS IN c AND d

- d convolutions have simple four-lobe structure.
- In c left most satellite has 8 lobe with central blank.
- Others in c may or may not be similar.

FIGURE 10

CONVOLUTIONS WITH SQUARE APERTURES

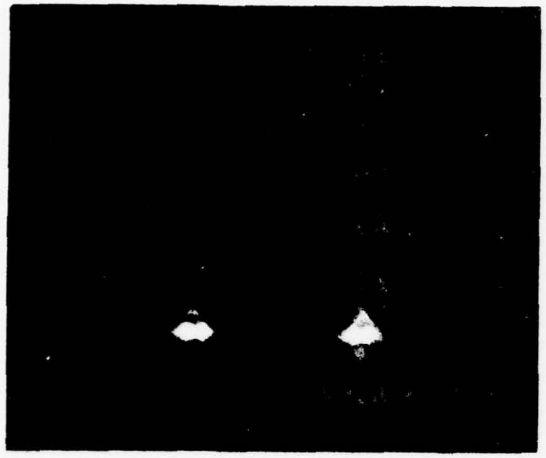

a.

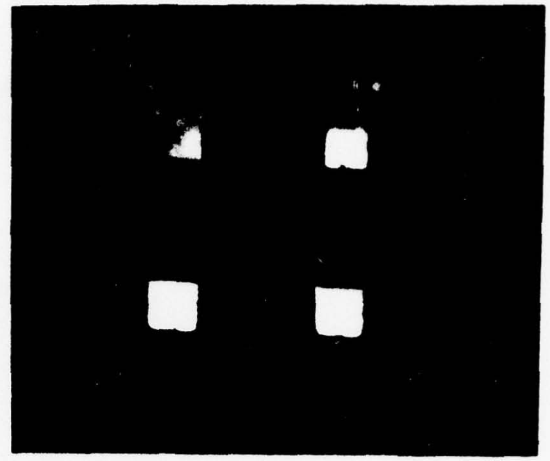

c.

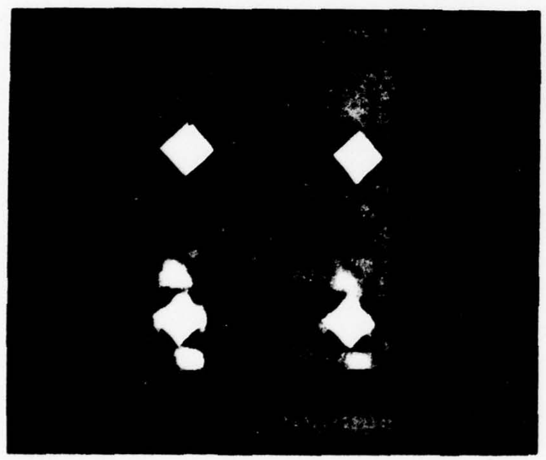

b.

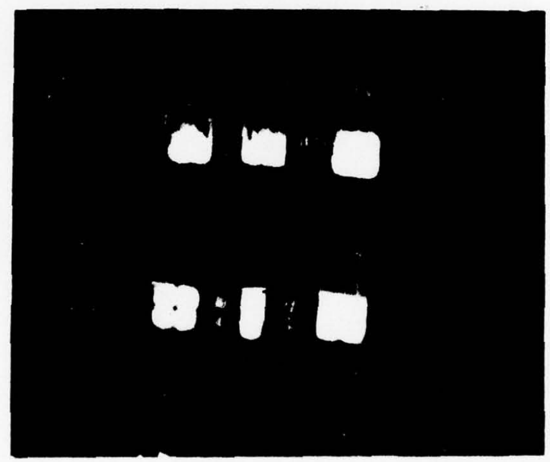

d.

EFFECT OF FILTERS ON TWO CRYSTAL EXPERIMENTS

CAPTION

(As Shown)

COMMENTS

- Green at input plane gives image plane hole radius.
- Intensity at image plane is total intensity.
- Red filter at object plane removes input plane green leaving upconverted A^2 intensity.
- Ratio of two proportional to normalized convolution intensity.
- Useful when evaluating system operation.

FIGURE 11

EFFECT OF FILTERS ON TWO CRYSTAL EXPERIMENTS

No Filter

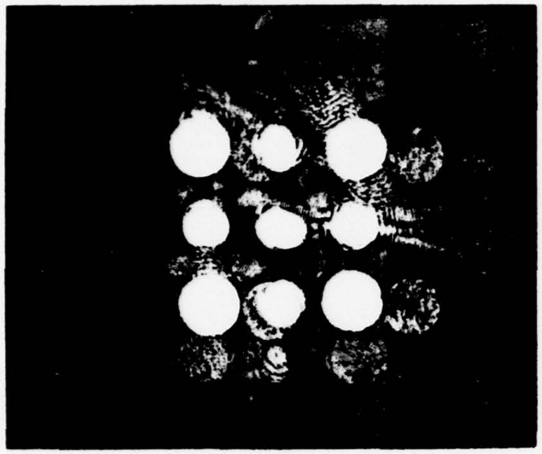

a. High Speed Film

Red Filter

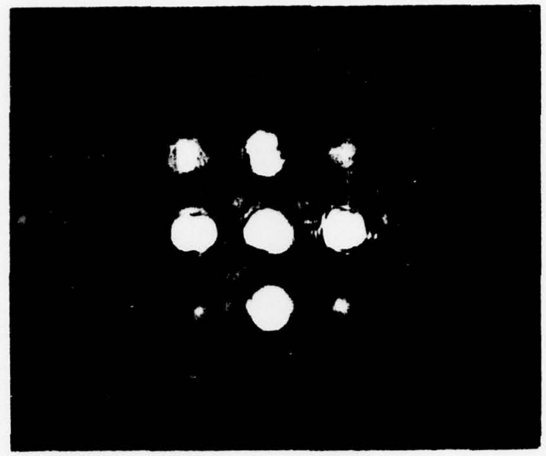

b. High Speed Film

Red Filter

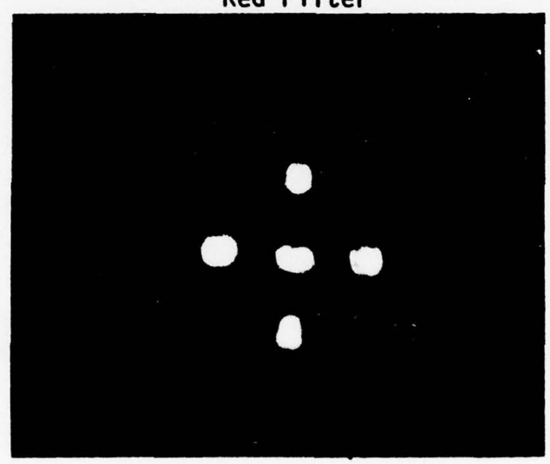

c. Low Speed Film

INTERNAL REFLECTIONS AND SHG

<u>CAPTION</u>:

<u>a</u>. Type 52 <u>b</u>. Type 57. <u>c</u>. Type 57 ; 3 pulses.

<u>d</u>. Two crystals, no filter, 4 pulses.

<u>e</u>. Two crystals, red filter at object plane, 4 pulses.

<u>COMMENTS</u>:

WEAKER INTENSITY REFLECTIONS IN <u>a</u>, <u>b</u> AND <u>c</u> APPEAR WITH INCREASING EXPOSURE.

- A^2 convolutions much stronger than auto-λ-convolutions.
- Diagonal auto-λ-convolution weakest of normal 5 <u>SHG</u> generated peaks.
- Reflection peaks stronger than auto-λ-convolutions.

REFLECTIONS IN TWO CRYSTAL EXPERIMENT <u>c</u> AND <u>d</u>

- Lower left green peak reflections in <u>c</u> correlated to co-located convolution peaks in <u>d</u>.
- Lower right peaks not related to reflected green incident at input plane.

POSSIBLE SOLUTIONS TO REFLECTIONS

- Non-parallel crystal faces.
- Index matching fluid.
- Absorption filters in SHG Housing.

FIGURE 12

INTERNAL REFLECTIONS AND SHG

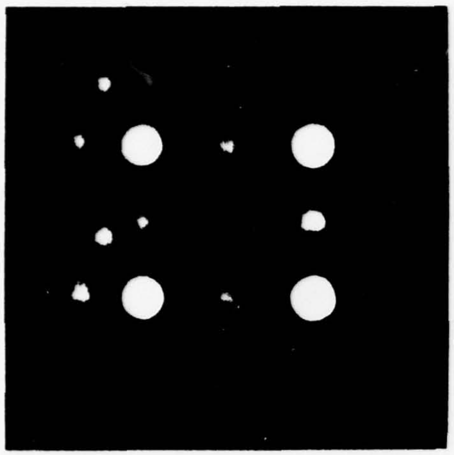

a

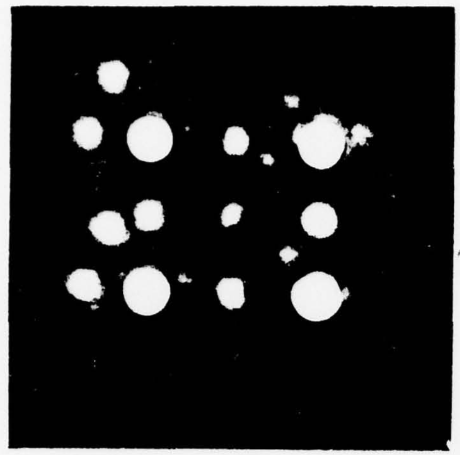

b

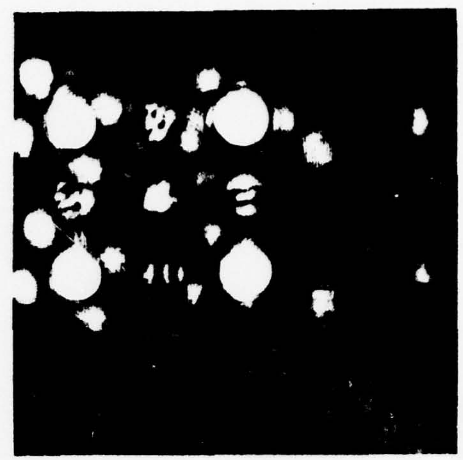

c

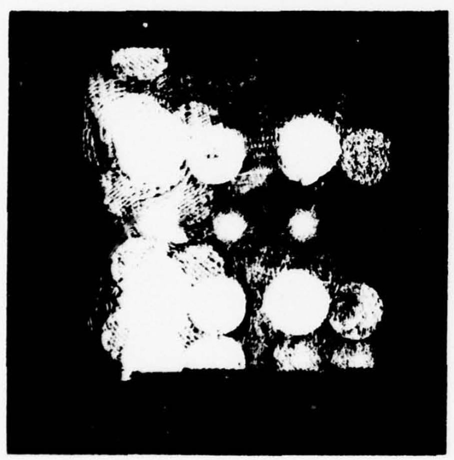

d.

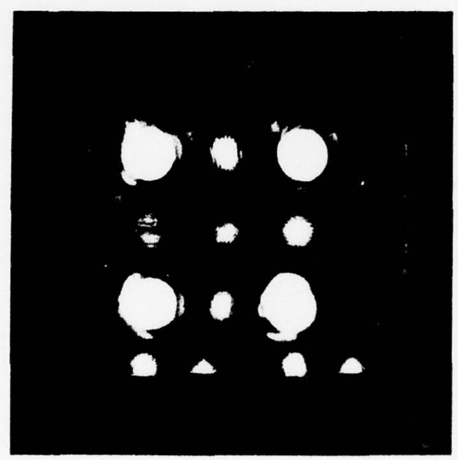

e.

SIMULTANEOUS AUTO-CONVOLUTIONS, A^2-CONVOLUTIONS AND NOISE

CAPTION:

a, b, c exposed with λ_1 on object plane.

d and e exposed with *both* λ_1 *and* λ_2 *on object* plane.

Mask used in a, c and e.

COMMENTS:

A^2 convolutions in all 5 exposures.

Auto-convolutions in b partly hidden by noise related to left object in a.

FIGURE 13

SIMULTANEOUS AUTO-CONVOLUTIONS, A^2-CONVOLUTIONS AND NOISE

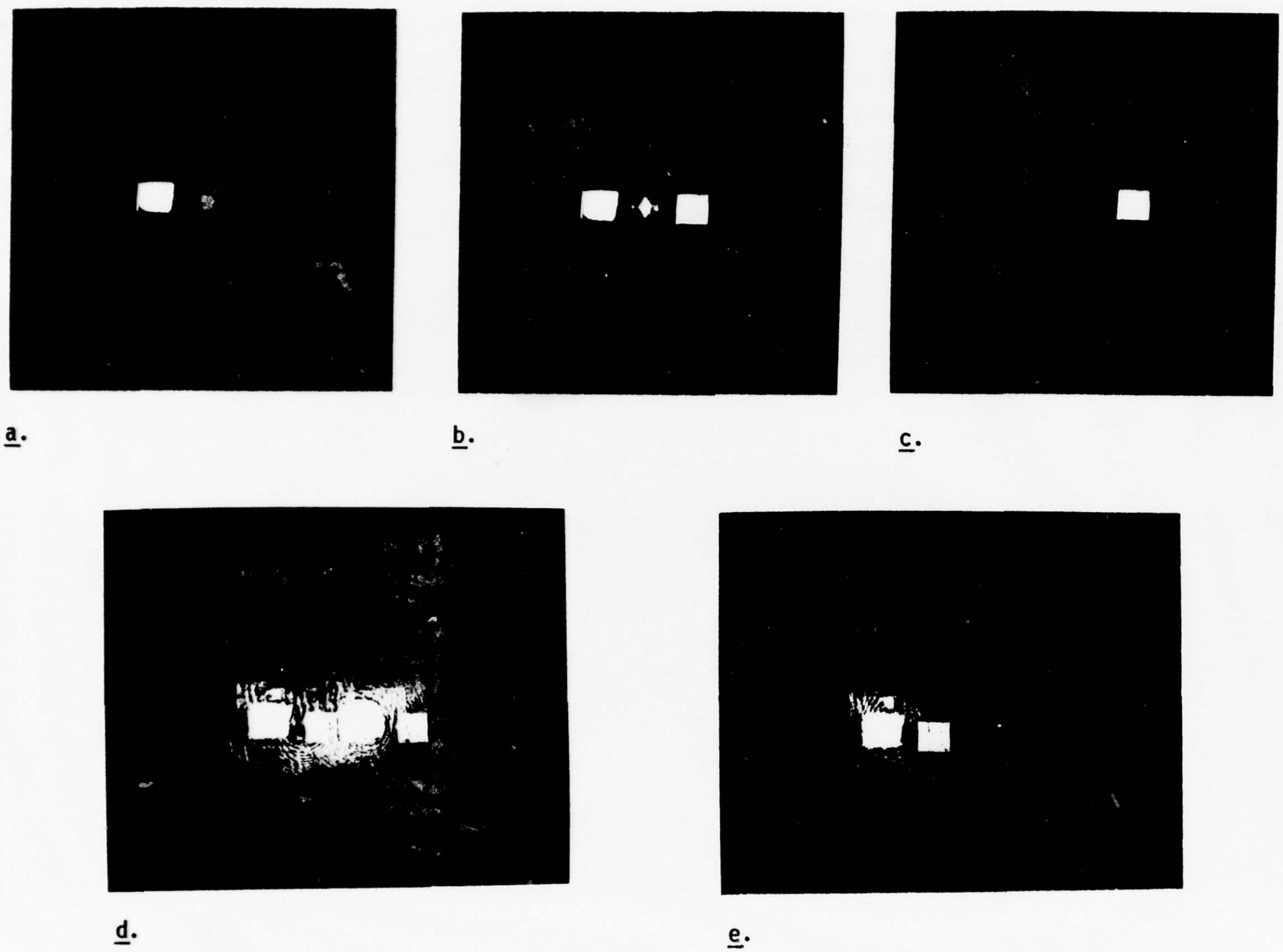

CONVOLUTION NON-LINEARITY

CAPTION:

ALL OBJECT PLANES ILLUMINATED BY FUNDAMENTAL (λ_1)

a and b also illuminated by 2nd Harmonic (λ_2)

a illuminated by 1 pulse.

c and d illuminated with 2 pulses.

b illuminated with 3 pulses.

c convolution observed during crystal warmup.

COMMENTS:

NON-LINEARITY OF CONVOLUTION OPERATION.

- A^2-convolutions very bright in upper half: White in top half > white in bottom half.
- Auto-convolution in c also brighter in top half.

FIGURE 14

CONVOLUTION NON-LINEARITY

a

b

c

d

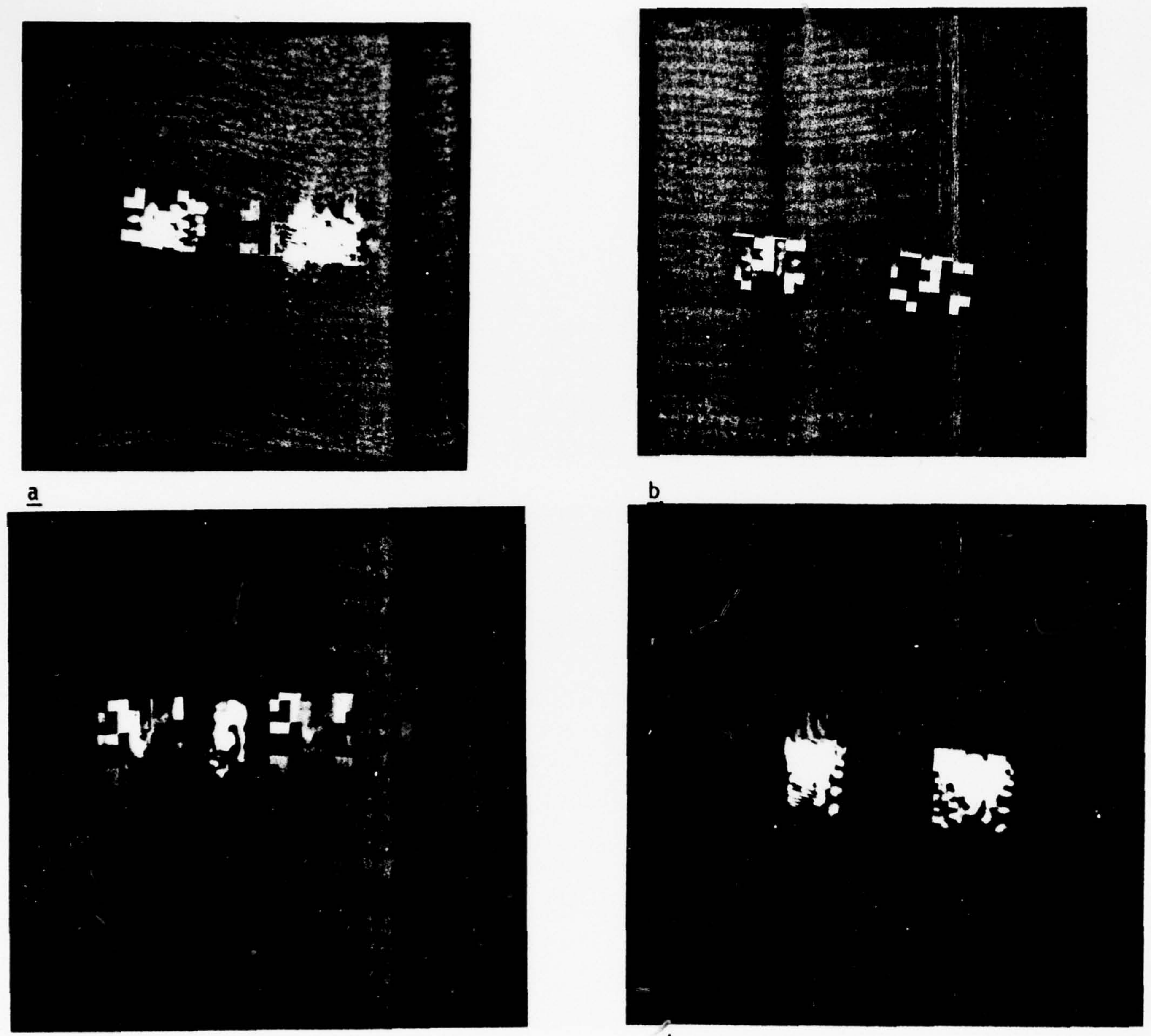

a b c d

FIGURE . CONVOLUTIONS.

VARIATION IN A^2-AND AUTO-CONVOLUTION PEAK INTENSITY RATIOS

CAPTION:

a. and b. are two different settings of FP crystal.

c. same setting as b. except using Polaroid Type 57 film instead of Type 52.

COMMENTS:

NOW UNDERSTOOD AS VARIATIONS OF FP CRYSTAL

- Angle relative to optic axis.
- Temperature.
- Longitudinal position.

ANOTHER FACTOR IS RELATIVE FOCAL LENGTHS BETWEEN CONVOLUTION f AND g

- $n(\lambda_f) \neq n(\lambda_g)$
- Object plane not perpendicular to optical axis.

FIGURE 15

VARIATION IN A^2- AND AUTO-CONVOLUTION PEAK INTENSITY RATIOS

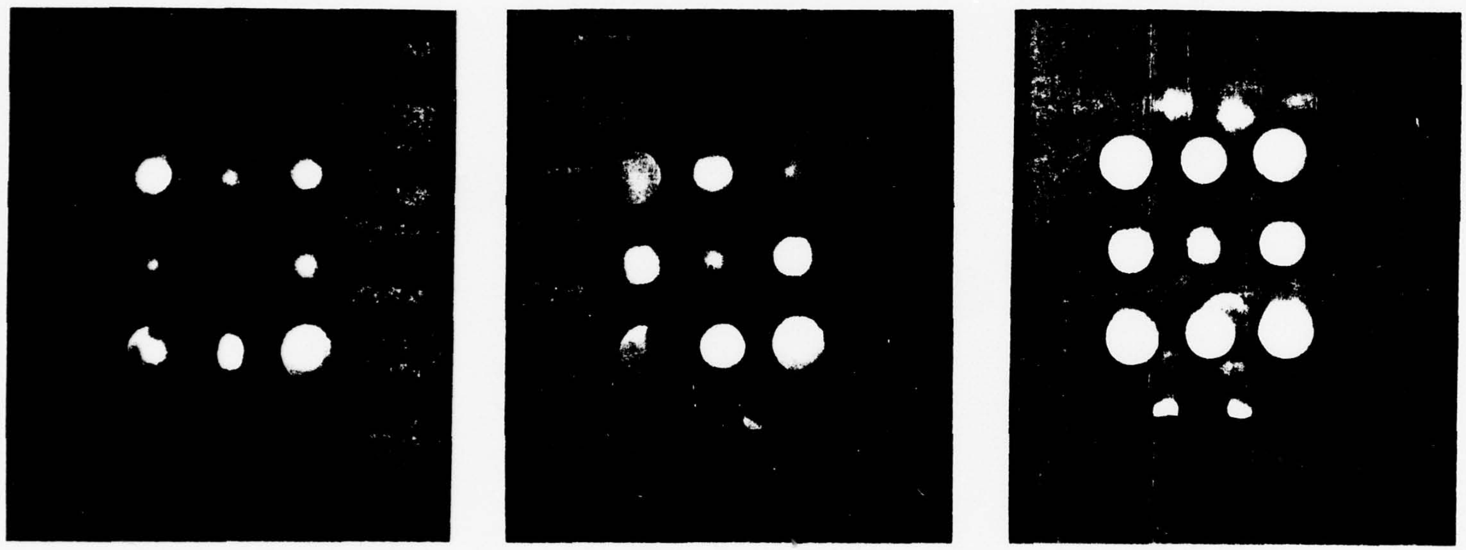

a b c

FP PLANE CRYSTAL: TEMPERATURE EFFECTS

CAPTION:

PROBABLY POLAROID TYPE 57

COMMENTS:

INCREASE OF 10°C (from a to b).

- Vertical and horizontal auto-λ-convolutions saturated.
- Diagonal auto-λ-convolution disappears.
- A^2-convolution increase (? - possible IR effect).

SIMILAR CONCLUSIONS APPLY TO c AND d.

FIGURE 16

FP PLANE CRYSTAL TEMPERATURE CRYSTALS

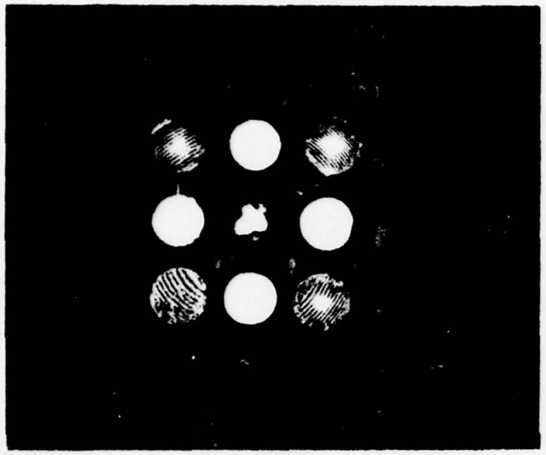

50°C

a.

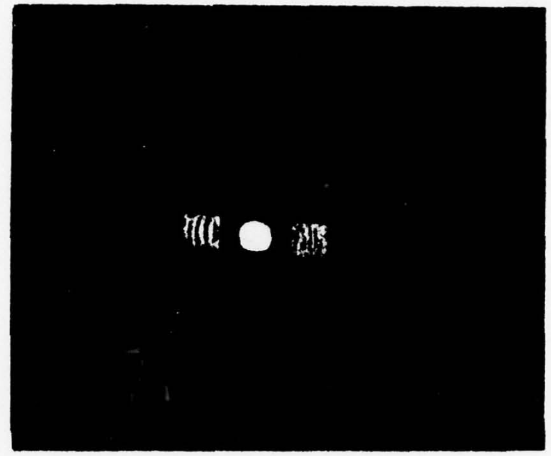

c.

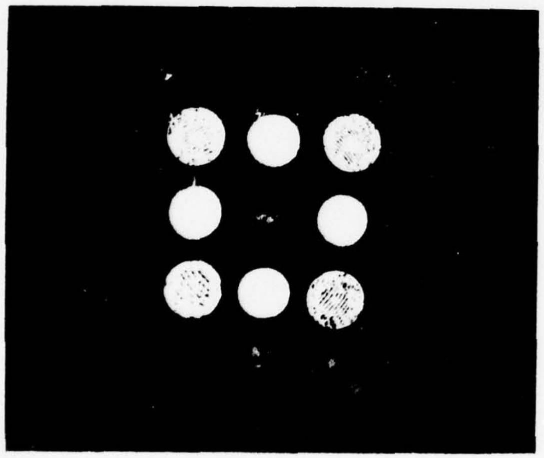

60°C

b.

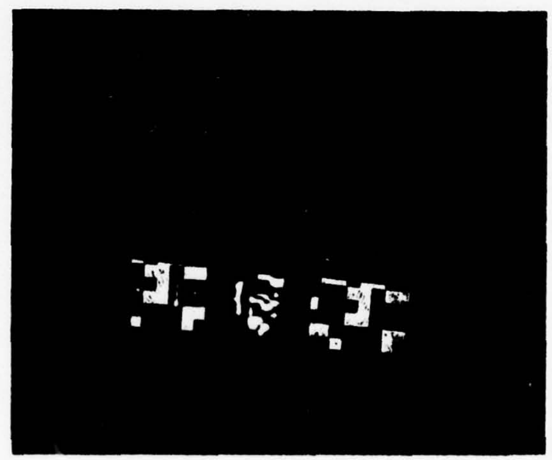

d.

A^2-CONVOLUTION VARIATION WITH LONGITUDINAL IMAGE PLANE LOCATION

<u>CAPTION</u>:

(None)

<u>COMMENTS</u>:

HIGH SPATIAL FREQUENCY SENSITIVITY TO LONGITUDINAL IMAGE-PLANE LOCATION.

- Auto-λ-convolution spectrum insensitive.
- A^2-convolution related high frequency spectrum is sensitive (seen with top aperture in <u>b</u> and lower right aperture in <u>c</u>).

CONCLUDE LATTER RELATED TO FP CRYSTAL DAMAGE

- Shows insensitivity of convolutions to crystal damage.
- Could be used to probe 3 dimensional damage in crystals.
- Can be inverted to model effects of crystal damage on system degradation.

FIGURE 17

A^2-CONVOLUTION VARIATION WITH LONGITUDINAL IMAGE PLANE LOCATION

1 Pulse 4 Pulses 4 Pulses

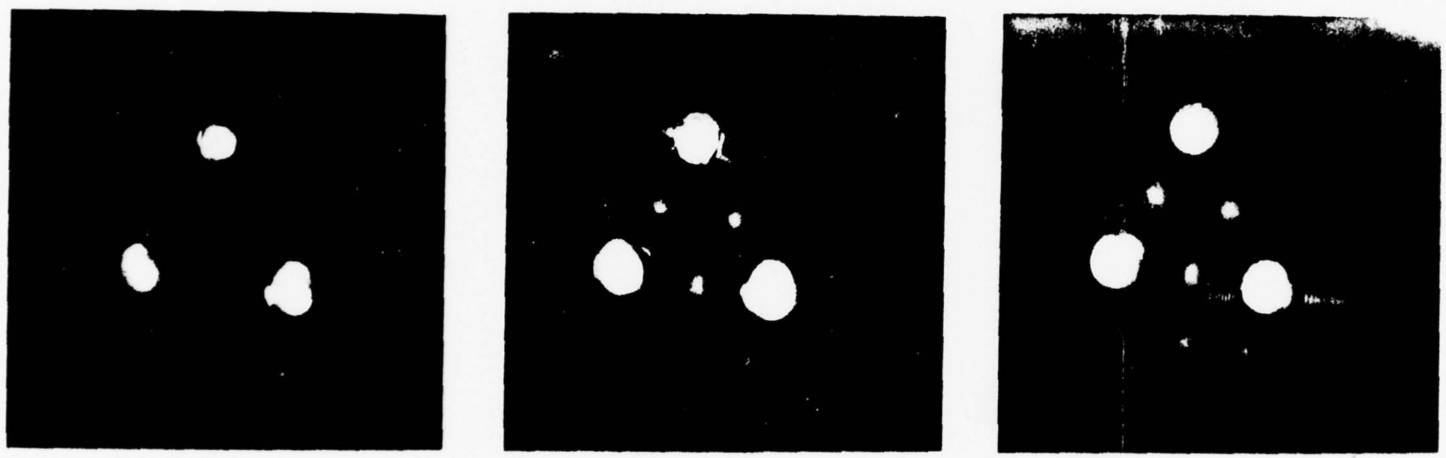

a. b. c. $\Delta Z(I) = -4.5$ cm

N-TEST OF CD*A AT 25°C

CAPTION:

a. Type 55, 1 pulse.
b. Type 55, 5 pulses.
c. Type 57, 1 pulse.
d. Type 52, 1 pulse.
e. Type 57, 1 pulse.
Red input plane filter used with d and e.

COMMENTS:

A^2-CONVOLUTIONS OF EACH LINE

- Difference in total length gives minimum separation of convolving points to upconvert.
- Other features noted without further analysis:

  Lines are segmented (e.g.: left vertical line in d).

  Higher harmonics (e.g.: left vertical line in e).

AUTO-λ-CONVOLUTIONS

- Wishbone shape.
- Higher harmonics also wishbone shaped.
- Joint of wishbone bisects angles between parallels and diagonal of N.
- Arms of wishbone are complex interaction between intersection angle of converging light cones at different temperatures.

NOISE RELATED TO KNOWN CRYSTAL DAMAGE

FIGURE 18

N TEST OF CD*A AT 25°C

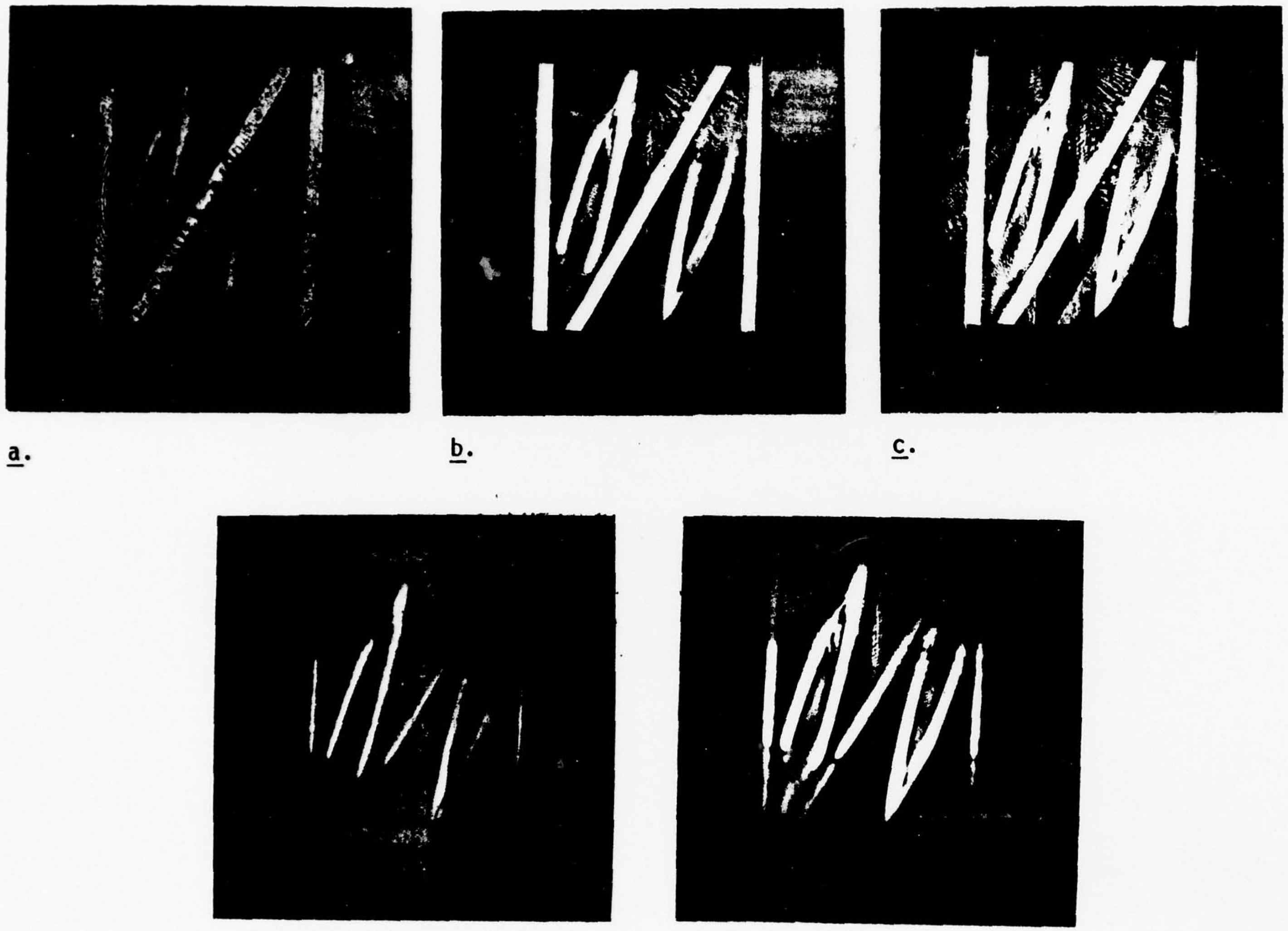

a. b. c. d. e.

N-TEST OF CD* A AT 50°C

<u>CAPTION</u>:

All Type 57 High Speed Film.

<u>a</u> & <u>c</u>. 1 Pulse Exposure.

<u>b</u> & <u>d</u>. 5 Pulse Exposure.

<u>c</u> & <u>d</u>. Red input plane filter used.

<u>a</u> & <u>b</u>. Rotated 90° c-clockwise from orientation of <u>c</u> & <u>d</u>.

<u>COMMENTS</u>:

(SEE COMMENTS FOR D12)

WITH INCREASE OF 25°C:

- Wishbone moves toward apexes of N-arm intersections.
- Effects on wishbone angle and width not analyzed.
- Shape insensitive to rotation to 1<u>st</u> order approximation.

FIGURE 19

N-TEST OF CD*A AT 50°C

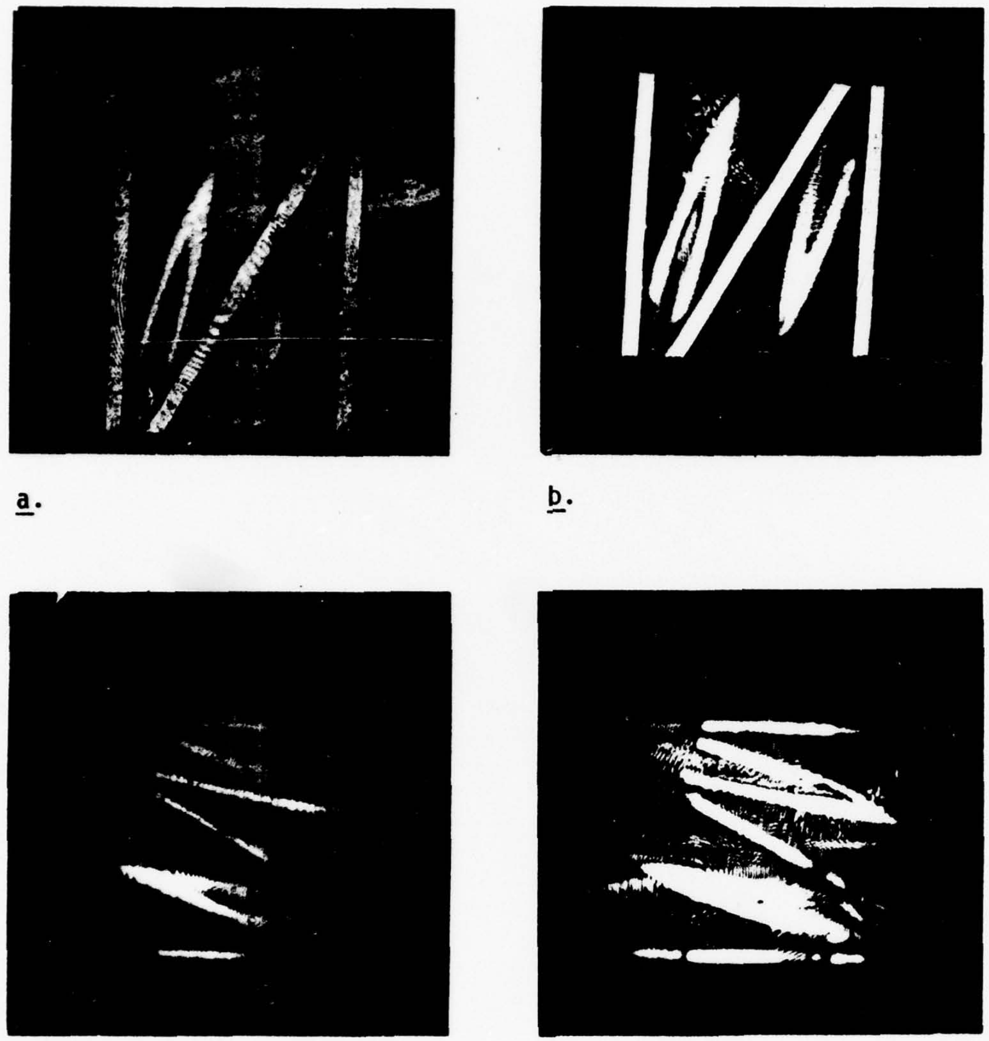

a. b. c d

N-TEST OF CD*A AT 75°C

CAPTION:

All Film Type 55 PN

a & c. 5 pulse exposure

b & d. 1 pulse exposure

c & d. Red input plane filter used

COMMENTS:

- (SEE COMMENTS FOR D-12 AND D-13).
- WISHBONE MOVES FURTHER TOWARD N VERTICES.

FIGURE 20

N-TEST OF CD*A AT 75°C

a

b

c

d

N-TEST OF CD*A AT 100°C

CAPTIONS:

SEE FILM TYPE 55 PN.

a. 1 pulse exposure.

b. 3 pulse exposure.

c. 5 pulse exposure using red input plane filter.

COMMENTS:

- (SEE COMMENTS FOR D-12, D-13 AND D-14)
- Only junction of wishbone remains.
- Higher harmonics of wishbone conjugate to those in 25°C have appeared.

FIGURE 21

N-TEST OF CD^*A AT 100°C

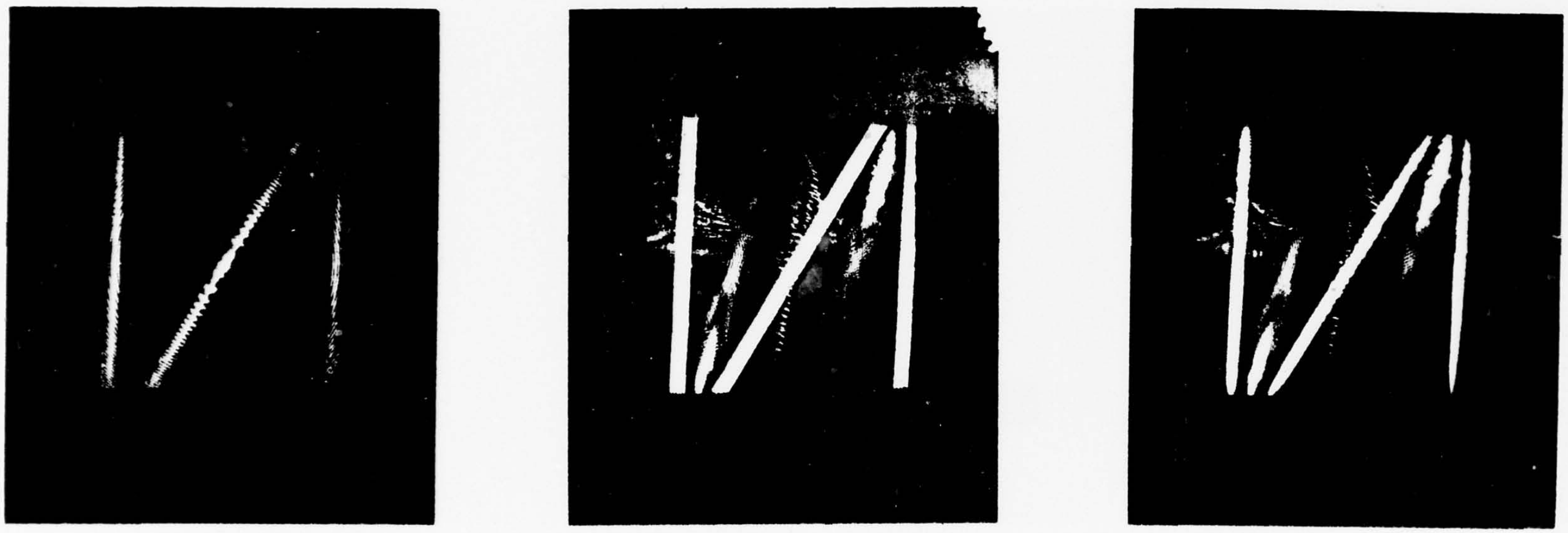

a. b. c.

ANGLE AND TRANSLATION EFFECTS ON CD*A SHG

CAPTION:

N-Test Configuration

a, b, and c. oriented at reference angle.

d. Rotated +0.83°.

a. Reference height of CD*A crystal.

b. And d moved up 2 mm.

c. Moved up 1 mm more (Δh=3mm)

COMMENTS:

- Intensity decreases with increased height near bottom of crystal.
- Intensity decreases sharply as h (c) approached.
- Angle tuning improves intensity: b to d.
- Crystal volume damage noise changes as crystal translated.

FIGURE 22

ANGLE AND TRANSLATION EFFECTS ON CD*A SHG

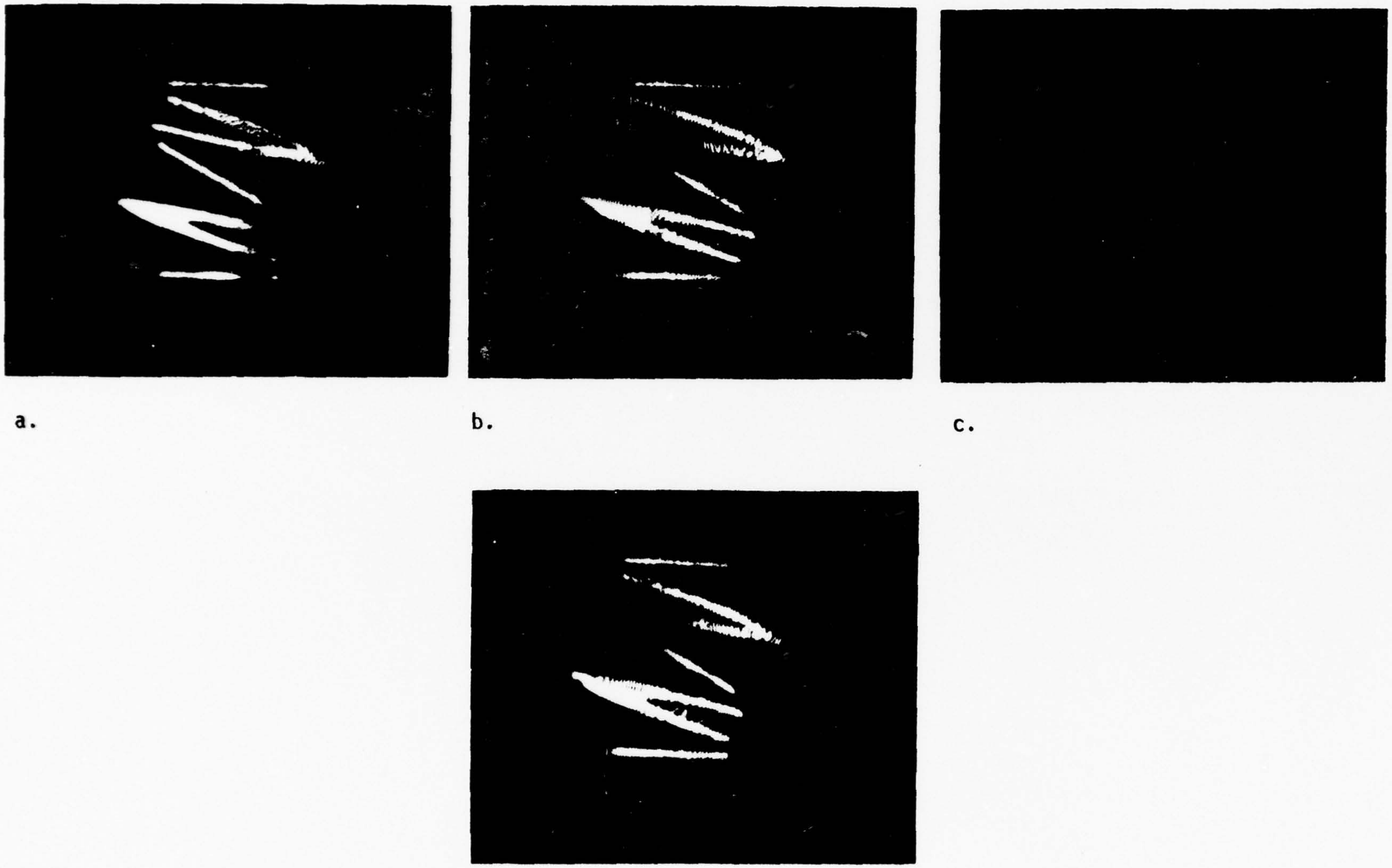

a. b. c.

d.

AUTO-λ-CONVOLUTIONS WITH CD*A CRYSTAL AT 25°C

<u>CAPTION</u>:

Object plane illuminated using λ_1 and λ_2 in <u>a</u>, <u>b</u>, and <u>c</u>.

Red filter absorbed λ_2 in front of object plane in <u>d</u>, <u>e</u> and f.

Pairs <u>a</u> and <u>d</u>, <u>b</u> and <u>e</u>, and <u>c</u> and <u>f</u> show exposures of same subject without and with filter.

Fourier filter crystal temperature is 25°.

<u>COMMENTS</u>:

Only auto-λ-convolution observed midway between object plane subjects for T = 25°.

FIGURE 23

AUTO- λ -CONVOLUTIONS WITH CD^*A AT 25°C

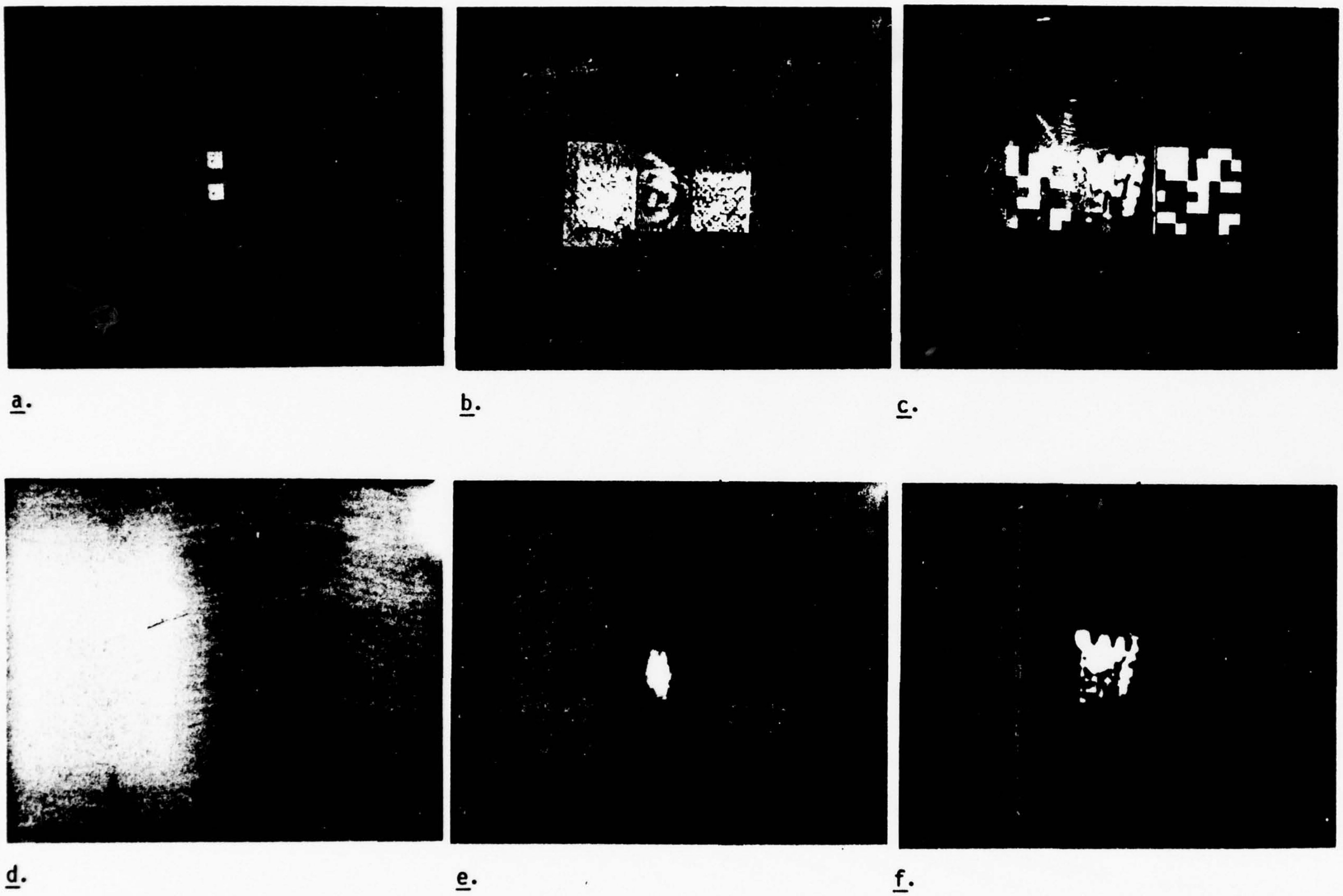

CONCLUSIONS

ORIGINAL CONTRACT (RETROSPECTIVE W/O P.G.)

- TOO AMBITIOUS EXCEPT FOR "BEST EFFORT"
- NOT DEFINITIVE ENOUGH: DEPENDED ON
  - FIRST TRY OPERATION
  - HeNe READOUT OF ZERO-FIELD (MODIFY)
  - FINDING METHOD TO DOWN CONVERT.

ACCOMPLISHMENTS

- EVALUATED DIGITAL & JTC FILM BASED DATA. NEED OPTICAL CONVERSION TO COMPLETE
- PURCHASED AND ASSEMBLED LASER AND CRYSTAL
- SINGLE FREQUENCY UPCONVERSION: READY
- 3 FREQ UPCONVERSION: HAVE SMALL TEST CRYSTAL
- N-TEST DEMONSTRATED UP AND DOWN CONVERSION: T, λ
- READY TO CONSIDER RUBY LASER READOUT OF DC FIELD

RECOMMENDATION

FINISH SINGLE FREQUENCY UPCONVERSION EXPERIMENT WITH COMPLEX CONJUGATES

- USE NRL BIT SHIFTED DATA
- EXPERIMENTAL/THEORETICAL STUDY: 2 FREQUENCIES UP/DOWN CONVERSIONS

  BOTH TEMPERATURE AND ANGLE TUNING (MODIFIED N-TEST)

  RESOLUTION VS ANGULAR WIDTH OF EACH IMAGE

  RESOLUTION VS INTERSECTION ANGLE 2 IMAGES

ADDITIONAL TOPICS TO CONSIDER

- RUBY LASER READOUT OF "ZERO FREQ" CORRELATION FIELD
- 2 CRYSTAL DOWNCONVERSION CORRELATION: IMAGE SCALING
- FOR COMPLETENESS: REPRODUCE RUSSIAN 3 CRYSTAL UP/DOWN CONVERSION

APPENDIX A-II

THEORY

A-II.1 The Convolution and Correlation Operations

The convolution and correlation of two input functions can easily be formed in an optical system. This is done by using the Fourier transform properties of lenses and the square law effect of an intensity sensitive material or a nonlinear device. The correlation function is of particular interest since it is used in many image identification and related data processing operations.

The convolution of the function f(x) with g(x) is given by

$$h(x) = f \times g = \int_{-\infty}^{\infty} f(u)\, g(x - u)\, du. \qquad (1\text{-}1)$$

One way of interpreting this is to envision the function g being reversed and slid along f, as shown in Figure A-1. The convolution h(x) is then found to be the product of f with g when g is centered at x. This product is the shaded area shown in the diagram. The new weighted distribution is a smoothed version of the original.

One exercise that is useful as a mental check on the calculated convolution is summarized in Figure A-2. Imagine that one of the functions is plotted backwards on a movable piece of paper. For the exponential functions used here the product will be zero when the paper is to the left of the position shown. The product slope then suddenly rises to some maximum value, where the rate of overlap of the two functions is large. As the reversed function moves to the right of this position, the convolution rises to a maximum and it finally falls off to zero.

The correlation function differs in that the second function is not reversed when calculating the product area. The two operations are the same, then, only if the input functions are symmetric. Unlike the convolution, the correlation function often results in a peaked distribution. This is especially true when one function is similar to the other. This peaked portion is due to the large

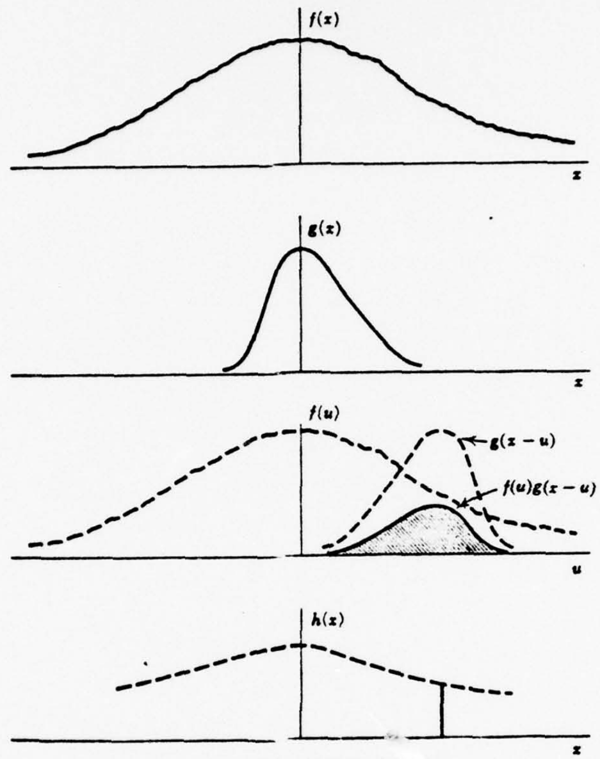

Figure A-1. The convolution integral h(x) = f(x) * g(x) represented by a shaded area.

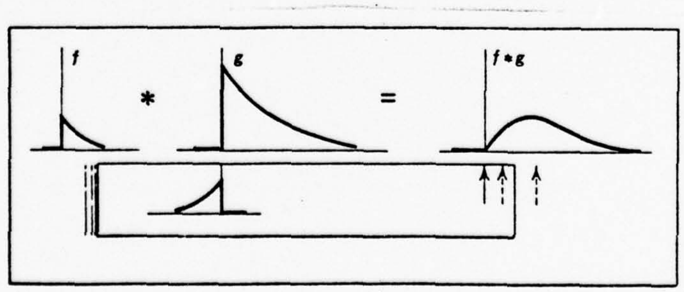

Figure A-2. Graphical construction for convolution. The movable piece of paper has a graph of one of the functions plotted backward.

area of overlap that occurs when the functions are similar. The cross-correlation function is given by the expression

$$f * g = \int_{-\infty}^{\infty} f(u)\, g^*(u - x)\, du$$

$$= \int_{-\infty}^{\infty} f^*(u)\, g(u + x)\, du. \qquad (1\text{-}2)$$

This function, being a measure of similarity is a maximum when f = g (this is the "autocorrelation" of f with itself).

The formation of the convolution and correlation products are also found by Fourier transforming operations by making use of the relationships below. Capital letters are used here to denote the Fourier transform of a given function (i.e., $G = F\left\{g\right\}$).

convolution:

$$g \otimes h = F\left\{G(u)\, H(u)\right\} = F\left\{G(u)\, H^*(-u)\right\} \qquad (1\text{-}3)$$

correlation:

$$g * h = F\left\{G(u)\, H^*(u)\right\} \qquad (1\text{-}4)$$

Because the pseudo random codes studied in this contract are not symmetric, the correlation and convolution operations will not be the same. In order to determine bit shift then, a difference frequency correlation configuration must be used if nonlinear crystals such as CD*A are used.

To correlate two images with these crystals, a joint transform correlator can be used. Here the input functions are positioned a focal length distance f in front of a Fourier transforming lens. The Fourier domain lies a distance f behind this lens. The spatial frequencies that exist in the input function will be displaced from each other here. They will lie at a distance

$$X = f_x\, \lambda f \qquad (1\text{-}5)$$

in the Fourier plane. Here f_x is the frequency component in question, λ is the optical processing wavelength and f is the focal length of the Fourier transforming lens.

After the transforms are mixed by the square law effect of the crystal, the product is inverse transformed by a second lens. According to Equation (4), this yields the correlation.

For the case where nonlinear crystals are used to mix the Fourier domain components, the output will appear at a different λ than used to illuminate the input. The color of the correlation peak will be the difference frequency of the input.

The spatial extent required of the nonlinear crystal is governed by Equation (1-5) and the dimensions of the input imagery. For example, assume that 50 bit/cm density codes are to be correlated. In order to obtain a well resolved correlation peak, frequency components several times this value must be processed. For a large gain, let us require that six times the fundamental frequency be processed. Using Equation (5), the minimum crystal width is found:

$$\begin{aligned} x &= (6 \times 50 \text{ bits/cm})\ (1.06 \times 10^{-4} \text{ cm})\ (33.02 \text{ cm}) \\ &= 1.04 \text{ cm} \end{aligned} \tag{1-6}$$

Since CD*A crystals are not grown much larger than this 1 cm, a maximum bit density of 50 bits/cm must be used. To process data beyond this, some modification of the joint transform correlation configuration must be made.

By moving the input plane along the optical axis, the size of the Fourier transform can be continuously varied. Table A-1 summarizes the effects of input plane position on the phase and scale terms that appear with the actual transform. If the input function is positioned a distance d from the output plane, then the transform will be scaled by d, instead of f. Since $d<f$, the transform will be smaller, and the width required of the CD*A crystal will not be as extensive. A phase term will also be introduced, but will be

cancelled when the correlation product is formed. In this modified system, therefore, the maximum bit density that can be tolerated at the input will be determined by the crystals size and resolution.

Table A-1

Source position	Object position (relative to lens)	Output plane	Phase term	Scale proportional to
∞	f in front	f behind	—	f
∞	z_1	f behind	$\frac{x^2(-z_1)}{2f^2}$	f
∞	0	f behind	$x^2/2f$	f
∞	behind lens distance d from output plane	f behind	$x^2/2d$	d
p	f in front	$z_2=\left(\frac{p-f}{pf}\right)^{-1}$	—	f
p	z_1	$z_2=\left(\frac{p-f}{pf}\right)^{-1}$	$\frac{x^2(f-z_1)}{2[z_2(f-z_1)+fz_1]}$	$\frac{z_2(f-z_1)+fz_1}{f}$
p	0	$z_2=\left(\frac{p-f}{pf}\right)^{-1}$	$x^2/2z_2$	z_2

A-II.2 Frequency Conversion

In certain classes of crystals it is possible to mix optical radiation in order to generate sum and difference frequencies. When coherent light of only one wavelength is available, the input frequency is doubled and the difference frequency term is zero. Thus, harmonic generation can be used to extend the frequency range of available laser sources. Active or passive parametric upconversion can also be used for detecting an IR reflected or emitting scene. The IR radiation is imaged onto the nonlinear upconverting crystal. A "pump" laser then floods the IR scene in the crystal. Interaction between the IR and pump laser radiation produces the sum of the two frequencies and a visible image output is produced.

For our application here the nonlinear dielectric properties of these crystals are used to produce an output distribution that is proportional to the square of the incident field. This phenomena allows us to obtain the convolution or correlation of two input images, when the crystals are used within the Fourier domain of the system.

Let us look at this frequency conversion operation in more detail. When a material is subjected to a weak electromagnetic field, the induced polarization is linear inside the media. When higher optical field strengths are present, such as those available from laser sources, higher order responses are induced. Of particular interest is the second order polarization in which the sum or difference frequencies of two incident fields at $\omega_1 \pm \omega_2$ are produced. The new polarization can be written as

$$P_i(\omega_1 \pm \omega_2) = g\, \varepsilon_o \sum_{J,K=1,2,3} d_{ijk}\,(-\omega_1 \pm \omega_2, \omega_1, \pm \omega_2)\, E_{\omega_1} E_{\omega_2} \qquad (2\text{-}1)$$

Here g is a degeneracy constant, d_{ijk} a third order tensor of nonlinear optical coefficients, and E_j, E_k the field amplitudes.

As a result of crystal symmetry, many of the components of d_{ijk} will often be zero or equal to other components of the crystal.

In order for this new optical field to propagate, it must travel at the same velocity as the incident fields. If this condition is not met, the electromagnetic radiation created by a dipole at one point will not couple to that created elsewhere and destructive interference will occur. In general, because of normal dispersion this propagation velocity is different at the sum and difference frequency than it was for the incident fields. The efficiency of conversion is therefore a function of the phase mismatch

$$\Delta k = \vec{k}_{\omega_1 \pm \omega_2} - \vec{k}_{\omega_1} - \vec{k}_{\omega_2} \qquad (2\text{-}2)$$

The wave vectors are equal to $\vec{k}_i = \vec{u}_i \, (2\pi/\lambda n)$, where $\vec{u}$ is a unit propagation vector.

One technique used to satisfy the phase-matching requirement $\Delta k - 0$ is to take advantage of the natural birefringence of anisotropic crystals. To see how this is done consider an ellipsoid with major axes in the x, y and z directions. This "index ellipsoid" can then be used to find the two allowed directions of polarization and the indices for these directions. This is done as follows. Through the center of the ellipsoid a plane is drawn perpendicular to the direction of propagation. The intersection of this plane and the ellipsoid is an ellipse. The two axes of this ellipse are parallel to the two directions of polarization, and the length of each is equal to twice the refractive index in that direction.

If all three major axes of the index ellipsoid are unequal, then the crystal is called biaxial, since two optic axes can be defined. An optic axis is the wave-normal direction in which the refractive index is independent of the direction of polarization (the direction perpendicular to a circular cross section of the ellipsoid).

Uniaxial crystals are more commonly encountered. The direction of polarization perpendicular to the optic axis is known as the ordinary direction. The index is independent of the direction of propagation for such an "ordinary" wave. For the other direction of polarization, the extraordinary direction, the index changes elliptically between the value of the ordinary index n_o, when the wave

normal is parallel to the optic axis, and the extraordinary index n_e, when the wave normal is perpendicular to the optic axis. When the wave normal is in a direction θ to the optic axis the extraordinary index is given by

$$n_e(\theta) = \frac{n_e\, n_o}{(n_o^2 \sin^2\theta + n_e^2 \cos^2\theta)^{1/2}} \tag{2-3}$$

Using angle tuning or temperature tuning of these anisotropic crystals, the phase matching requirement can be met.

Consider, for example, the case of second harmonic generation. Using Equation (2-2) it can be seen that $\Delta k = 0$ if $n^{2\omega} = n^{\omega}$. In normally dispersive materials the index of the ordinary wave or the extraordinary wave along a given direction increases with ω. This makes it impossible to satisfy the condition $n^{2\omega} = n^{\omega}$ when they are both extraordinary or ordinary. Consider, however, a crystal with $n_e^{2\omega} < n_o^{\omega}$. An angle θ_m then exists at which $n_e^{2\omega}(\theta_m) = n_o^{\omega}$; if the fundamental beam (at ω) is launched along θ_m as an ordinary ray, the second-harmonic beam will be generated along the same direction as an extraordinary ray. This situation is illustrated in Figure A-3. The angle θ_m is found at the intersection between the index surface of the ordinary beam at ω (circle) to the index surface of the extraordinary ray. This gives $n_e^{2\omega}(\theta)$. Using Equation (2-3), for negative uniaxial crystals (those for which $n_e^{\omega} < n_o^{\omega}$) θ_m is found to be

$$\sin^2\theta_m = \frac{(n_o^{\omega})^{-2} - (n_o^{2\omega})^{-2}}{(n_e^{2\omega})^{-2} - (n_o^{2\omega})^{-2}} \tag{2-4}$$

It is seen that the angle at which the wave vectors propagate determine the phase mismatch. These, and other physical parameters of the system, can be used along with Maxwell's equations to solve for the intensity of the upconverted wave. If depletion of the fundamental wave is neglected and Δk assumed constant throughout the crystal, then the conversion efficiency is given by

$$\frac{P_{SH}}{P_R} = 2\left(\frac{\mu_o}{\epsilon_o}\right)^{3/2} \omega_1^2 \frac{d_3^2 \ell^2}{n^3} \operatorname{sinc}\left(\frac{\Delta k \ell}{2}\right) \frac{P_\omega}{A} \tag{2-5}$$

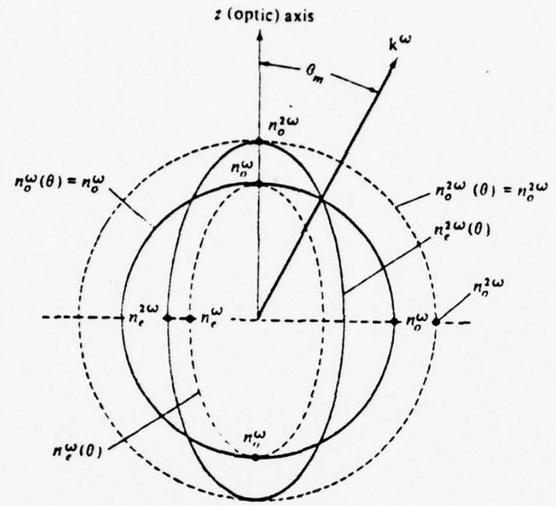

Figure A-3. Normal (index) surfaces for the ordinary and extraordinary rays in a negative ($n_e < n_o$) uniaxial crystal. If $n_e^{2\omega} < n_o^{\omega}$, the condition $n_e^{2\omega}(\theta) = n_o^{\omega}$ is satisfied at $\theta = \theta_m$. The eccentricities shown are vastly exaggerated.

The phase mismatch Δk due to interference is seen to reduce efficiency by the factor sinc $\left(\frac{\Delta k \ell}{2}\right)$. The efficiency is also found to be proportional to the intensity P_ω/A of the fundamental beam.

So far we have seen that by proper orientation a crystal can be positioned such that the refractive index at a frequency ω is equal to the refractive index at 2ω. Second harmonic generation can thus be achieved at an angle θ. Because the angle at which $n_e^{2\omega}(\theta) = n_o$ varies with wavelength, this angle will differ for different incident frequencies. There is one disadvantage to this angle tuning technique. Because the beams involved do not propagate along the principal axis of the crystal, the ordinary and extraordinary beams diverge. This limits the interaction length, and hence crystal efficiency.

An alternate means of phase matching a crystal is by temperature tuning. This can be done since the extraordinary index is more temperature dependent than the ordinary index. This 90° phase matching is satisfied by orientating

the crystal at 45° to both the X and Y direction, and perpendicular to the optic axis. The incident beam is polarized along the X-Y plane, the generated frequency along Z. These 90° phase matched and angle tuning orientations are shown in Figure A-4 below.

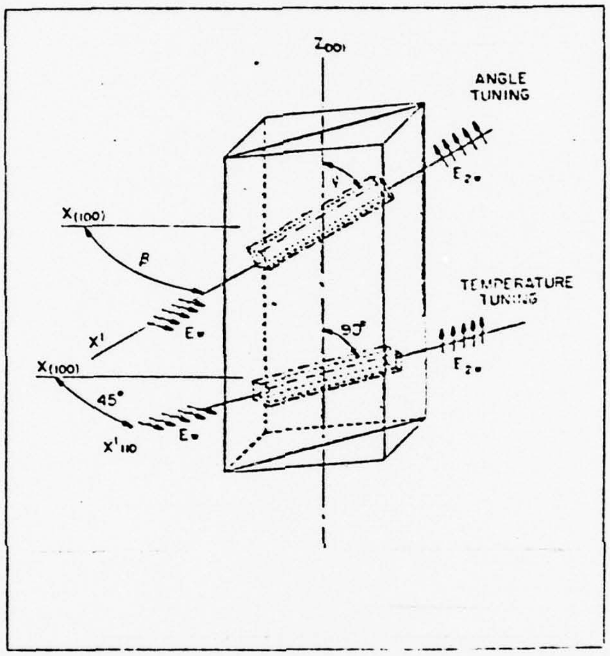

Figure A-4. Crystallographic orientations for angle and temperature tuning.

By looking at the phase mismatch versus θ, the acceptance angle of a particular configuration can be computed. In general, $\Delta\vec{k} = 0$ only for one direction of the incoming beams. As rays come in from angles other than this, $\Delta\vec{k}$ becomes nonzero. This results in a decrease in efficiency which in turn limits the field angle.

As an example, consider a type I interaction in which two ordinary rays, $\vec{k}_p$ and $\vec{k}_{ir}$ intermix to form the sum frequency $\vec{k}_s$. The angular deviation of the signal in the plane of the wave vectors (parallel case) can then be found:

$$(\Delta\theta_{\parallel})^2 \cong \frac{2\Delta k}{k_{ir}\left(1 - \frac{k_{ir}}{k_s}\right)} \qquad (2\text{-}6)$$

Likewise, the acceptance angle in a direction perpendicular to the plane of the wave vectors (perpendicular case) can also be found by wave vector analyses. vector analyses. In the small angle approximation it is seen that

$$\Delta\theta_{\perp} \cong \frac{2\Delta k}{k_{ir}\left(1- \frac{k_{ir}}{k_s}\right)} \tag{2-7}$$

In general, it can be seen that an extensive analysis is required to find the field of view for a particular system. The phase match angle and temperature are first found for the central beams of the reference and signal beams to be correlated. The indices of refraction for these beams are then found. This gives a numeric value to the wave vectors k_{ir}, k_p and k_s. An alternate experimental procedure is to use the N-pattern Test (Appendix A-1, Section 4.10) to fix some of the parameters and then complete the calculation analytically.

The maximum allowable phase mismatch is assumed to be $\Delta k = 2\pi/L$. It is noted that a shorter crystal is preferable to increase the field of view. A shorter crystal, however, decrease the interaction length and hence decreases efficiency. Some optimum value must be found. With the parameters k_{ir}, k_p, k_s and Δk, the field angle can be found.

A-II.3 Soviet Papers

In the work done by MDAC this year, the convolution of input imagery was obtained. This was done by using the frequency doubling properties of non-linear crystals. Theoretically, the correlation can also be obtained. To do this a difference frequency mode of operation must be used. Since Soviet papers have been published which show the generation of difference frequency harmonics, these results will be used to compare to our predictions.

Figure (A-5) shows the results published by R. Eremeeva (Reference 1). In Figure (A-5), the input data is shown separated by a distance "a".

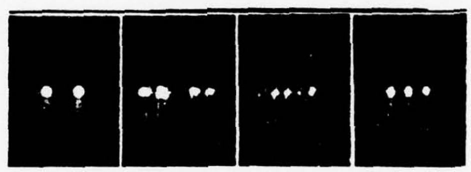

a b c d

Figure A-5. Soviet Data

The remaining figures show the results of using different combinations of input illumination. In Figure (A-5b) a neodymium laser at λ_1 and its third harmonic (λ_3) are used; in Figure (A-5c) λ_1 and λ_2 are incident on the input images. The difference frequency correlation is recorded at the output. In Figure (A-5d) the convolution is found by recording the second harmonic of λ_1.

To mathematically describe the input functions, let g_1 and g_2 be written in complex notation form. Hence,

$$\begin{aligned} E_{in} &= \frac{1}{2}\left(g_1(x-a)e^{-j\omega_1 t} + g_1^*(x-a)e^{j\omega_1 t}\right) \\ &+ \frac{1}{2}\left(g_2(x+a)e^{-j\omega_1 t} + g_2^*(x+a)e^{j\omega_2 t}\right) \end{aligned} \quad (3\text{-}1)$$

The phase factors are used to describe what input wavelengths illuminate the two functions since $\omega_i = 2\pi C/\lambda_i$. A Fourier transform is next taken of this input. The scale and shift properties of this operation are taken into account. At the Fourier plane, the distribution

$$E_F = \frac{1}{2}\left[G_1(u)e^{-jua}e^{-j\omega_1 t} + G_1^*(u)e^{-jua}e^{j\omega_1 t} + G_2\left(\frac{\lambda_1}{\lambda_2}u\right)e^{-j\frac{\lambda_1}{\lambda_2}ua}e^{-j\omega_2 t} + G_2^*\left(\frac{\lambda_1}{\lambda_2}\right)e^{-j\frac{\lambda_1}{\lambda_2}ua}e^{j\omega_2 t}\right] \quad (3\text{-}2)$$

is formed.

After passing through the nonlinear crystal, this field is squared. It is then inverse transformed by a final lens. This output is found to be

$$\begin{aligned} 2E_0 = {} & R_{11}*\delta(x,\omega) + R_{2'2}*\delta(x',\omega) \\ & + \frac{1}{2}\left(C_{11}*\delta(x-2a,\omega+2\omega_1)\right) \\ & + \frac{1}{2}\left(C_{2'2'}*\delta(x'-2a,\omega+2\omega_2)\right) \\ & + C_{12'}*\delta\left(x-a+\frac{\lambda_1}{\lambda_2}a,\omega+\omega_1+\omega_2\right) \\ & + R_{12'}*\delta\left(x+a+\frac{\lambda_1}{\lambda_2}a,\omega+\omega_2-\omega_1\right) \\ & + \text{conjugate terms.} \end{aligned} \quad (3\text{-}3)$$

The letters R and C stand for the correlation and convolution operations, respectively. The primed numbers are used to take into account the λ_1/λ_2 scale factor that occurs when the input imagery is illuminated with different wavelengths. For example, the second to last term indicates that the correlation of $g_1(x)$ is made with $g_2(\lambda_1/\lambda_2 x)$. This term will appear at a spatial location $x = -(a + \lambda_1/\lambda_2 a)$, and at a temporal frequency of $(\omega_1-\omega_2)$. The "δ" notation is used to convey this information. The conjugate terms mentioned in this equation are those which are obtained when the +, -, 1, and 2 signs are replaced with -, +, 2 and 1, respectively.

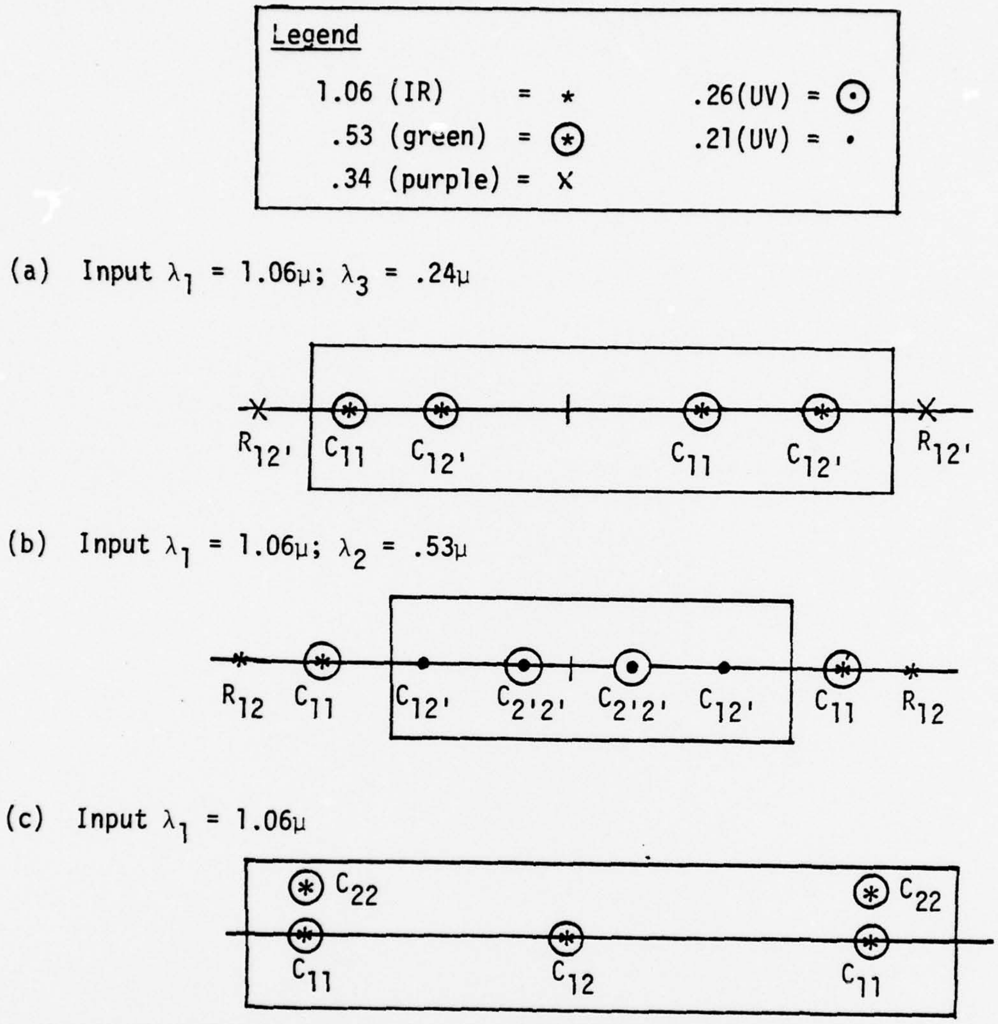

Figure A-6. Predicted Output Data for Various Combinations of Input Illumination. The Enclosed Data is Postulated to Have Been Photographed for Figure (4).

This equation can now be compared to the experimental results. To do this, the different terms are plotted in Figure (A-6). For example, λ_1 and λ_3 are used as inputs. At the output, four convolution terms appear in green, and a correlation function appears in violet. The term "oscillating at $2\omega_3$" will not appear since this is beyond the response of the available detectors. The four functions in green are those that appear in the Soviet data of Figure (A-5b).

When λ_1 and λ_2 are used as the processing wavelengths, then the output data appears as in Figure (A-5b). Now four convolution functions appear in the UV, one in green and a correlation term appears at 1.06μ. Since the Soviet data of Figure (A-5c) contain four terms, it is assumed that their data are a photograph of the UV terms (only black and white reprints are available for our analysis).

If only one wavelength is present at the input ($\lambda_1 = \lambda_2$), then Equation (3-3) reduces to terms at the three spatial locations x=0, $\pm$. This result has been verified experimentally in our lab and also appears in Figure (A-5d). It is seen that only convolution terms are present. The correlation term is frozen in time since the difference frequency $(\omega_1 - \omega_2) = 0$. Two-frequency illumination is therefore preferred if correlation data is of interest.

A-II.4 Determination of Bit Shift

It is desirable to determine the number of bits that one coded sequence is shifted with respect to a second. This is accomplished by using the position of the correlation peak at the output of the optical processor.

The codes to be processed have been sent to us from NRL. According to them, the patterns used are generated using a "random number generator that is essentially a 31 bit linear shift register with feedback taps to yield a maximal length pseudo random sequence. Such a generator yields in excess of 2×10^9 bits before repeating." The codes are recorded in raster format into an M x M array.

A total of b bits are then dropped, and this new bit shifted code is recorded to the right of the reference code.

A-II.4.1 Correlation of Zero-Bit Shifted Imagery

The correlation of two bit images can be predicted by decomposing each image into the sum of its individual bits. For example, let g be the M x M reference array composed of the bits g_{ij}. Then

$$g = \sum_{i=1}^{M} \sum_{j=1}^{M} g_{ij} \qquad (4\text{-}1)$$

Similarily, let the second image be defined as

$$h = \sum_{k=1}^{M} \sum_{\ell=1}^{M} h_{k\ell} . \qquad (4\text{-}2)$$

The correlation of the two images is then given by the transformed product

$$\begin{aligned} g * h &= F^{-1} \left\{ GH^* \right\} \\ &= F^{-1} \left\{ \left(\sum_i \sum_j G_{ij} \right) \left(\sum_k \sum_\ell H^*_{k\ell} \right) \right\} \end{aligned}$$

$$= F^{-1}\left\{\sum_i \sum_j G_{ij}\, H_{ij}^{*}\, d^{j2\pi(u\Delta x \,+\, v\Delta y)}\right\} \qquad (4\text{-}3)$$

$$+ \text{ cross terms}$$

In the latter expression Δx and Δy are the separation, at the input plane, between the two bits of g and h of indices (i, j). Since the correlation of these bits overlap at the output plane, the other terms are much lower in intensity by comparison. These "noise" terms are therefore neglected.

After carrying out the inverse Fourier transform of Equation (4-3) the location of the correlation peak is found to be

$$g * h = \sum_{\ell=1}^{M} \sum_{j=1}^{M} g_{ij} * h_{ij} * \delta(x - \Delta x,\, y - \Delta y) \qquad (4\text{-}4)$$

For two M x M arrays spaced a distance "a" from each, define the coordinate system shown in Figure A-6.

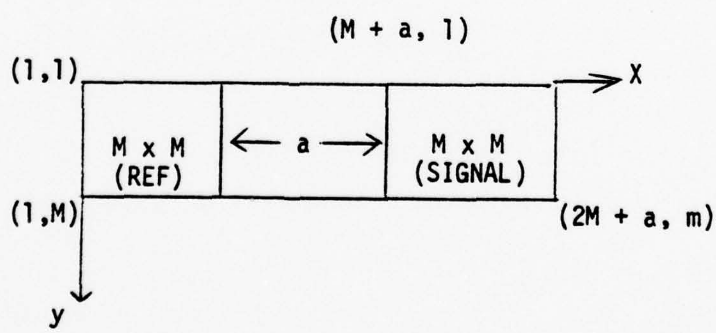

Figure A-6. Coordinate system for zero bit shifted array.

For this case $\Delta x = M + a$, $\Delta y = 0$. The correlation peak is therefore located at a relative output position of (m + a, 0),

AII.4.2 Correlation of Bit Shifted Images

Consider next the situation where a total of b bits have been dropped from the right hand image before it was recorded. In Figure (A-7) the new reference and signal images are depicted. The hatched area represents the bits that have been dropped to form the signal image. Areas numbered 1 and 2 are matched.

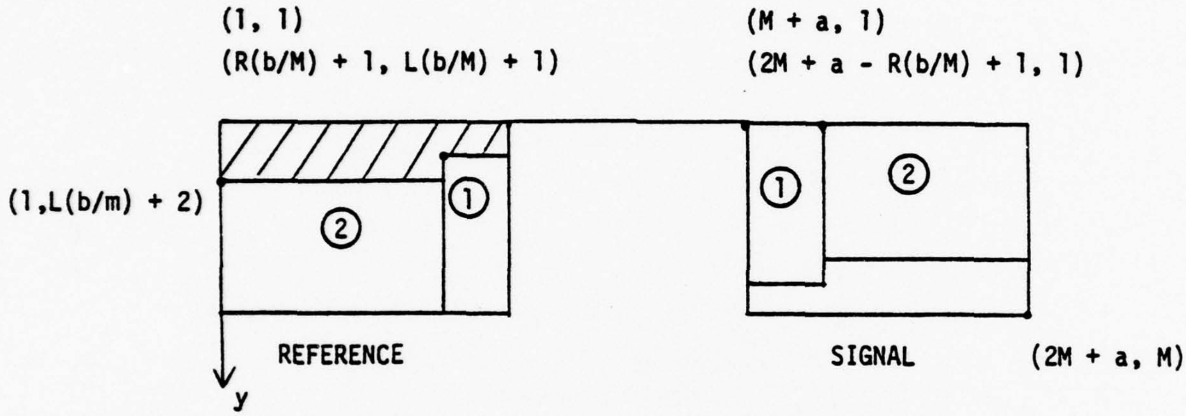

Figure A-7. Coordinates of 1st Bit of Matched Imagery Sections.

Using Equation (4-3) the location of the correlation peak is seen to be a function of the separation between matched data sections. To determine the values of Δx and Δy for the respective image sections, define the coordinate of the first bit (of reference) to be used in signal image as

$$(R(b/m) + 1, L(b/m) + 1) \tag{4-5}$$

Here the symbol "L" is used to denote the "floor" of the quotient $b \div m$, or the next smallest integer "R" is the remainder for this product. Coordinates are then assigned to the images.

The correlation of the bit shifted image can now be predicted:

$$g * h = (g_{①} * h_{①}) + (g_{②} * h_{②})$$

$$= g_{①} * h_{①} * \delta(M + a - R(b/M)-1, -L(b/M)$$

$$+g_{②} * h_{②} * \delta(2M + a - R(b/M), -L(b/M) -1)$$

(4-6)

The magnitude of these two terms will be proportional to the areas of images ① and ② , respectively.

As an example, consider the case of a 5 x 5 bit array where the first 7 bits have been dropped. The coordinates of the matched data sections are found by reference to Figure A-7. The initial coordinates of the first reference bit found in the signal is (R(b/M) +1, L(b/M) +1) = (R(7/5) + 1, L(7/5) + 1) = (3,2). The first coordinate of signal section No. 2 is (2M + a - R(b/M) + 1, 1) = (2.5 + a - R(7/5) + 1, 1) = (9 + 9, 1). This is shown in Figure A-8.

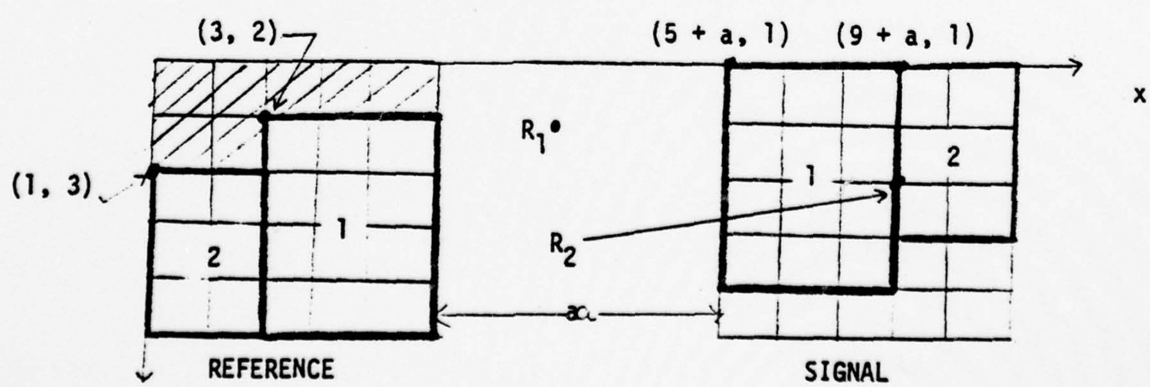

Figure A-8. Coordinates for 7 Bits Shifted on 5 x 5 Array.

From these values the spatial shifts Δx and Δy are found for the respective image sections. This shifts the correlation peak into the two positions given by Equation (4-5). In this case $g_1 * h_1$ is found at $R_1(2 + a, -1)$, and $g_2 * h_2$ at $R_2(8 + 9, -2)$. The locations of these two correlation points are also plotted in Figure A-8.

For the film-based correlations shown in Figure 4, Appendix A-I, a wrap-around format was used to form the bit-shifted signal. For this reason four images matched up with reference and four corresponding correlation peaks were formed.